AD-A145 798 SCATTERING FROM SNOW BACKGROUNDS AT 35 98 AND 140 GHZ (U) ROME AIR DEVELOPMENT CENTER GRIFFISS AFB NY D T HAYES ET AL. APR 84 RADC-TR-84-69 1/1

UNCLASSIFIED F/G 20/14 NL

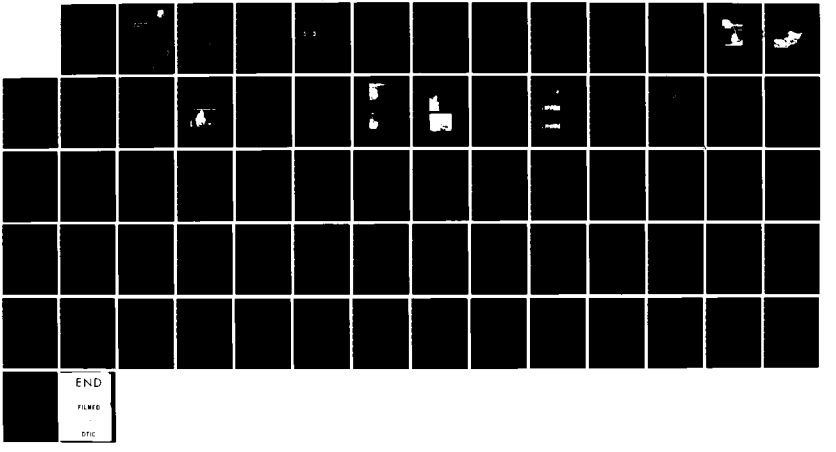

END

FILMED

DTIC

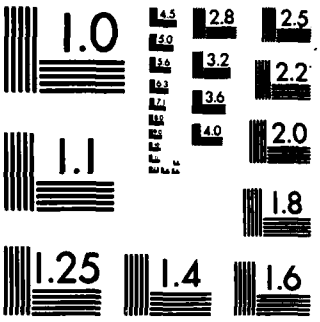

12

RADC-TR-84-69
In-House Report
April 1984

SCATTERING FROM SNOW BACKGROUNDS AT 35, 98, AND 140 GHz

Dallas T. Hayes
Uve H. W. Lammers
Richard A. Marr

ROME AIR DEVELOPMENT CENTER
Air Force Systems Command
Griffiss Air Force Base, NY 13441

This report has been reviewed by the RADC Public Affairs Office (PA) and is releasable to the National Technical Information Service (NTIS). At NTIS it will be releasable to the general public, including foreign nations.

RADC-TR-84-69 has been reviewed and is approved for publication.

APPROVED: John E Rasmussen

JOHN E. RASMUSSEN, Chief
Propagation Branch
Electromagnetic Sciences Division

APPROVED: Allan C Schell

ALLAN C. SCHELL
Chief, Electromagnetic Sciences Division

FOR THE COMMANDER: John A. Ritz

JOHN A. RITZ
Acting Chief, Plans Office

If your address has changed or if you wish to be removed from the RADC mailing list, or if the addressee is no longer employed by your organization, please notify RADC (EEPS) Hanscom AFB MA 01731. This will assist us in maintaining a current mailing list.

Do not return copies of this report unless contractual obligations or notices on a specific document requires that it be returned.

Unclassified

SECURITY CLASSIFICATION OF THIS PAGE

REPORT DOCUMENTATION PAGE

1a. REPORT SECURITY CLASSIFICATION Unclassified	1b. RESTRICTIVE MARKINGS
2a. SECURITY CLASSIFICATION AUTHORITY	3. DISTRIBUTION/AVAILABILITY OF REPORT Approved for public release; distribution unlimited.
2b. DECLASSIFICATION/DOWNGRADING SCHEDULE	
4. PERFORMING ORGANIZATION REPORT NUMBER(S) RADC-TR-84-69	5. MONITORING ORGANIZATION REPORT NUMBER(S)
6a. NAME OF PERFORMING ORGANIZATION Rome Air Development Center 6b. OFFICE SYMBOL (If applicable) EEP	7a. NAME OF MONITORING ORGANIZATION
6c. ADDRESS (City, State and ZIP Code) Hanscom AFB Massachusetts 01731	7b. ADDRESS (City, State and ZIP Code)
8a. NAME OF FUNDING/SPONSORING ORGANIZATION 8b. OFFICE SYMBOL (If applicable)	9. PROCUREMENT INSTRUMENT IDENTIFICATION NUMBER
8c. ADDRESS (City, State and ZIP Code)	10. SOURCE OF FUNDING NOS PROGRAM ELEMENT NO: 62702F; PROJECT NO.: 4600; TASK NO.: 16; WORK UNIT NO.: 07
11. TITLE (Include Security Classification) Scattering From Snow Backgrounds at (contd)	
12. PERSONAL AUTHOR(S) Hayes, Dallas T., Lammers, Uve H.W., Marr, Richard A.	
13a. TYPE OF REPORT Scientific 13b. TIME COVERED FROM _____ TO _____	14. DATE OF REPORT (Yr., Mo., Day) 1984 April 15. PAGE COUNT 66
16. SUPPLEMENTARY NOTATION	
17. COSATI CODES FIELD / GROUP / SUB. GR.	18. SUBJECT TERMS (Continue on reverse if necessary and identify by block number) Millimeter wave propagation; Snow Backscatter Terrain scatter; Free-water content

19. ABSTRACT (Continue on reverse if necessary and identify by block number)

Potentially, millimeter wave systems operating near terrain interact strongly with snow cover. The dependence of the millimeter-wave backscatter coefficient on physical snow parameters, such as metamorphic state and free-water content, were explored. The results complement a previous study done on dry slabs removed from snow cover (RADC-TR-81-88).

Low-power cw scatterometers at frequencies of 35, 98, and 140 GHz allowed backscatter measurements on in-situ snow at vertical, horizontal, and crossed polarization. Backscatter coefficients reported here were obtained by averaging returns while the scatterometer antenna footprints swept over the snow in a continuous circular motion. Grazing angles on the surface, constant during a sweep, were parametrically changed from 90 deg to 45 deg to 15 deg. The measurements took place in March 1978, late during that winter, when the snow cover was usually melting during the day and refreezing during the night. Melting-water calorimetry provided the free-water data. The snow depth on _

20. DISTRIBUTION/AVAILABILITY OF ABSTRACT UNCLASSIFIED/UNLIMITED ☒ SAME AS RPT. ☒ DTIC USERS ☐	21. ABSTRACT SECURITY CLASSIFICATION Unclassified
22a. NAME OF RESPONSIBLE INDIVIDUAL Dallas T. Hayes	22b. TELEPHONE NUMBER (Include Area Code) (617) 861-4264 22c. OFFICE SYMBOL EEP

DD FORM 1473, 83 APR EDITION OF 1 JAN 73 IS OBSOLETE.

Unclassified

SECURITY CLASSIFICATION OF THIS PAGE

BLOCK 11. (contd)

35, 98, and 140 GHz

BLOCK 19. (contd)

the ground exceeded 30 cm. It was composed of layers ranging from fresh to almost month-old granular snow.

Like-polarized backscatter coefficients of dry in-situ snow spread from a minimum of -12 dB at 35 GHz and 15-deg grazing angle to well over 0 dB at all frequencies (8 dB at 140 GHz) at 90-deg grazing angle. The cross-polarized backscatter coefficient, following the same trend, ranged from a low of -16 dB at 35 GHz and 15 deg to a high of 4 dB at 140 GHz and 90 deg. While in almost all cases like-polarized backscatter coefficients were lower for wet than for dry snow, the drop became less significant with higher frequency. At 140 GHz and perpendicular incidence, essentially no reduction was found. Cross-polarized backscatter coefficients of wet snow at 90-deg grazing angle ranged from a low of -25 dB at 35 GHz to a high of 2 dB at 140 GHz.

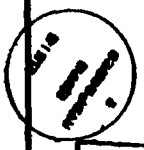

Contents

1. INTRODUCTION 7

2. THE IN-SITU BACKSCATTER PROGRAM 8

   2.1 Description of Scatterometer 9
   2.2 Measurement Procedures and Locations 11

3. GROUND TRUTH MEASUREMENTS 14

   3.1 Measurement Techniques 15
   3.2 Snow Conditions During Tests 16

4. DATA ANALYSIS 19

   4.1 Signal Fluctuation Rates 19
   4.2 Backscatter Statistics 25
   4.3 Backscatter Coefficients 31
   4.4 Comparison With Related Experiments 46

5. CONCLUSIONS 53

REFERENCES 55

APPENDIX A: Snow Data 57

Illustrations

1. Snow Scatterometer, In-Situ Backscatter Mode (Positioned for 90-deg Grazing Angle Measurements) 9

2. Snow Scatterometer, In-Situ Backscatter Mode (Positioned for 15-deg Grazing Angle Measurements) 10
3. Scatterometer Block Diagram 11
4. Image Source Calibration Procedure 12
5. Snow Trench Showing Collection of Ground Truth Data 14
6. View of Snow Surface on 11 March 1978 17
7. View of Snow Surface on 18 March 1978 17
8. View of Snow Surface on 20 March 1978 18
9. Closeup View of Larger Snow Grains of 20 March 1978 Shown on Millimeter Grid 18
10. Snow Backscatter Intensity (Raw Data of 18 March 1978, 35 GHz, Vertical Polarization, 90-deg Grazing Angle) 20
11. Snow Backscatter Intensity (Raw Data of 18 March 1978, 98 GHz, Vertical Polarization, 90-deg Grazing Angle) 20
12. Snow Backscatter Intensity (Raw Data of 18 March 1978, 140 GHz, Vertical Polarization, 90-deg Grazing Angle) 20
13. Scatterometer Positioned at Three Different Grazing Angles 21
14. Antenna Scanning Geometry 22
15. Backscatter Fluctuations (2 π-phase revolutions per degree of Scatterometer Rotation) vs Grazing Angle (Measured —— and Calculated - - -, Vertical Polarization) 24
16. Cumulative Probability of σ° PEAK ▲——▲ and σ° Δ - - - Δ (10 March 1978, 35 GHz, Vertical Polarization, 90-deg Grazing Angle) 26
17. Cumulative Probability of σ° PEAK ▲——▲ and σ° Δ - - - Δ (10 March 1978, 35 GHz, Vertical Polarization, 45-deg Grazing Angle) 27
18. Cumulative Probability of σ° PEAK ▲——▲ and σ° Δ - - - Δ (10 March 1978, 35 GHz, Vertical Polarization, 15-deg Grazing Angle) 28
19. Cumulative Probability of σ° PEAK (10 March 1978, 98 GHz, Vertical Polarization) 29
20. Cumulative Probability of σ° PEAK (10 March 1978, 140 GHz, Vertical Polarization) 30
21. σ° vs Grazing Angle (10 March 1978, 35 GHz; Dry Snow, Polarization VV D——D, HH D- - -D, HV D-.-.-D; Wet Snow, Polarization VV W——W, HH W- - -W, HV W-.-.-W; Free-Water Content 4.7 Percent) 33
22. σ° vs Grazing Angle (18 March 1978, 35 GHz; Dry Snow, Polarization VV D—D, HV D-.-.-D; Wet Snow, Polarization VV W—W, HH W- - -W, HV W-.-.-W; Free-Water Content 4.8 to 5.3 Percent) 34
23. Average of σ° for All In-Situ Data (35 GHz; Dry Snow, Polarization VV D—D, HH D- - -D, HV D-.-.-D; Wet Snow, Polarization VV W—W, HH W- - -W, HV W-.-.-W; Free-Water Content 3 to 15 Percent) 35
24. σ° vs Grazing Angle (10 March 1978, 98 GHz; Dry Snow, Polarization VV D—D, HH D- - -D, HV D-.-.-D; Wet Snow, Polarization VV W—W, HH W- - -W, HV W-.-.-W; Free-Water Content 5 Percent) 36

25. σ° vs Grazing Angle (18 March 1978, 98 GHz; Dry Snow, Polarization VV D—D, HH D- - -D, HV D-.-.-D; Wet Snow, Polarization VV W—W, HH W- - -W, HV W-.-.-W; Free-Water Content 7 to 9 Percent) 37

26. Average of σ° for All In-Situ Data (98 GHz; Dry Snow, Polarization VV D—D, HH D- - -D, HV D-.-.-D; Wet Snow, Polarization VV W—W, HH W- - -W, HV W-.-.-W; Free-Water Content 3 to 16 Percent) 38

27. σ° and Free-Water Content (FWC) vs Time of Day (In-Situ Data of 11 March 1978, 98 GHz, Vertical Polarization) 39

28. σ° and Free-Water Content (FWC) vs Time of Day (In-Situ Data of 11 March 1978, 98 GHz, Cross-Polarization) 40

29. σ° vs Grazing Angle (10 March 1978, 140 GHz; Dry Snow, Polarization VV D—D, HH D- - -D, HV D-.-.-D; Wet Snow, Polarization VV W—W, HH W- - -W, HV W-.-.-W; Free-Water Content 5 Percent) 42

30. σ° vs Grazing Angle (18 March 1978, 140 GHz; Dry Snow, Polarization VV D—D, HV D-.-.-D; Wet Snow, Polarization VV W—W, HH W- - -W, HV W-.-.-W; Free-Water Content 8 to 11 Percent) 43

31. Average of σ° for All In-Situ Data (140 GHz; Dry Snow, Polarization VV D—D, HH D- - -D, HV D-.-.-D; Wet Snow, Polarization VV W—W, HH W- - -W, HV W-.-.-W; Free-Water Content 3 to 11 Percent) 44

32. Average σ° vs Frequency, Grazing Angle of 90 deg (Dry Snow, Polarization VV D—D, HV D-.-.-D; Wet Snow, Polarization VV W—W, HV W-.-.-W) 45

33. Average σ° vs Frequency, Grazing Angle of 45 deg (Dry Snow, Polarization VV D—D, HV D-.-.-D; Wet Snow, Polarization VV W—W, HV W-.-.-W) 46

34. Average σ° vs Frequency, Grazing Angle of 15 deg (Dry Snow, Polarization VV D—D, HV D-.-.-D; Wet Snow, Polarization VV W—W, HV W-.-.-W) 47

35. Comparison of σ° Measured by University of Kansas at 35 GHz - - - With Our Average σ° for Dry Snow —— Taken From Figure 23 50

36. Comparison of σ° Measured by University of Kansas at 35 GHz - - - With Our Average σ° for Wet Snow —— Taken From Figure 23 51

Tables

1. E- and H-Plane Beamwidths of Transmitting and Receiving Antennas 23

2. Mean and Standard Deviation of Backscatter Coefficients for 35 GHz at $T < 0^\circ C$ 29

3. Mean and Standard Deviation of Peak Backscatter Coefficient for 98 GHz and 140 GHz at $T < 0^\circ C$ 31

Tables

4. Mean and Standard Deviation of Peak Backscatter Coefficient for $T > 0^{\circ}$ C at 90-deg Grazing Angle 31

5. Typical Values of σ° Measured at Grazing Angle of 15 deg by Georgia Institute of Technology[6] 48

A1. Physical Parameters of Snow Cover 10 March 1978 58

A2. Physical Parameters of Snow Cover 11 March 1978 59

A3. Physical Parameters of Snow Cover 13 March 1978 60

A4. Physical Parameters of Snow Cover 14 March 1978 61

A5. Physical Parameters of Snow Cover 18 March 1978 62

A6. Physical Parameters of Snow Cover 20 March 1978 63

A7. Free-Water Content of Snow Cover 10 March 1978 64

A8. Free-Water Content of Snow Cover 11 March 1978 65

A9. Free-Water Content of Snow Cover 18 March 1978 66

Scattering From Snow Backgrounds at 35, 98, and 140 GHz

1. INTRODUCTION

Millimeter waves penetrate the atmosphere well enough to be of interest for military system applications. *Advantages in size, resolution,* and *covertness* have stimulated the development of a large array of experimental hardware. Many of the required functions such as detection, guidance, and communication must be carried out in close proximity to terrain. Surface scatter, particularly from old, granular snow, constitutes an important interaction mechanism with terrain. Because of the nearly lossless dielectric properties of ice over the whole millimeter-wave range, and because of particle sizes of granular snow in the Mie region, efficient scattering has been observed over a wide range of grazing angles. Snow granules may act like Luneberg lenses. That is, scattering is highly directive toward the direction of incident radiation.

Past work on snow and ice scatter has been concerned mostly with longer microwaves.[1] Millimeter-wave data at small grazing angles[2] and at larger grazing

(Received for publication 17 April 1984)

1. Ulaby, F.T., Stiles, W.H., Dellwig, L.F., and Hanson, B.C. (1977) Experiments on the radar backscatter of snow, IEEE Trans. on Geoscience Electronics, GE-15 (No. 4):185-189.

2. Hoekstra, P., and Spanogle, D. (1972) Backscatter from snow and ice surfaces at near incident angles, IEEE Trans. on Ant. and Prop., AP-20 (No. 6):788-790.

angles[3,4,5] have been reported at 35 GHz. Some simultaneous measurements were performed at 35 and 95 GHz.[6] A good review of backscatter and attenuation properties of snow cover at frequencies of 35 GHz and below is contained in a report by Ulaby et al.[7]

In the RADC program, we measured millimeter-wave interaction with snow cover in the atmospheric window regions of currently greatest interest--35, 98, and 140 GHz. Initial results pertained to the scattering properties of frozen granular snow. Slabs of this type could be cut from snow cover and handled without breaking. A scatterometer/transmissometer was designed and built to make backscatter, bistatic scatter, and attenuation measurements on slabs. Data obtained in the slab mode were published in a companion report.[8]

Slabs could not be prepared from newly fallen snow or brittle snow. In addition, the effect of meltwater on the scattering properties could not be determined on slabs that had to be inverted from their natural position during measurement. Therefore, the investigation was extended to in-situ snow cover. The results of measurements at 35, 98, and 140 GHz on in-situ snow during the winter of 1977-78 are the subject of this report.

2. THE IN-SITU BACKSCATTER PROGRAM

The scatterometer employed for the in-situ measurements was a modified version of the device used for the snow-slab measurements. The basic design had been proven reliable during the slab measurements. Staying with the rugged and portable short-range system facilitated comparison between data obtained in both modes. The limited coverage of the scatterometer precluded wide-area mapping or imaging of snow-covered terrain. We considered this unimportant, since we were

3. Stiles, W.H., Hanson, B.C., and Ulaby, F.T. (1977) Microwave Remote Sensing of Snow, Experiment Description and Preliminary Results, University of Kansas RSL Tech. Rep. 340-1.
4. Ulaby, F.T., and Stiles, W.H. (1978) The Active and Passive Microwave Response to Snow Parameters. Part I: Wetness; Part II: Water Equivalent of Dry Snow, University of Kansas RSL Tech. Rep. 340-2.
5. Stiles, W.H., and Ulaby, F.T. (1980) Microwave Remote Sensing of Snowpacks, NASA Contr. Rep. 3263, Contract NAS5-23777.
6. Currie, N.C. (1977) Private communication.
7. Ulaby, F.T., Fung, A.K., and Stiles, W.H. (1978) Backscatter and Emission of Snow: Literature Review and Recommendations for Future Investigations, University of Kansas RSL Rep. 369-1.
8. Lammers, U.H.W., Hayes, D.T., and Marr, R.A. (1981) Millimeter Wave Scatter and Attenuation Measurements on Snow Slabs, RADC-TR-81-88, AD A112595.

mainly concerned with the generic scattering properties of the medium as a function of various microwave and meteorologic parameters.

2.1 Description of Scatterometer

The in-situ scatterometer is shown in Figure 1. It differs from the snow-slab

Figure 1. Snow Scatterometer, In-Situ Backscatter Mode (Positioned for 90-deg Grazing Angle Measurements)

version in that a sample holder is absent and the transmitters are relocated near the receiver front end at the upper end of the boom. The transmitter and receiver antennas point in almost parallel directions. Associated power supplies and other equipment on the sled structure act as counterweights to the weight of the boom. Rotating the upper part of the boom about the boom midpoint adjusts the grazing angle between antenna beams and snow surface. With the grazing angle fixed at a

particular value, the whole sled assembly rotates around its vertical axis. During such a scan, the scatter area on the snow surface describes a circular arc whose radius is a function of the grazing angle. The turntable on which the scatterometer rotates can also be seen in Figure 1. Equipment configurations for 90-, 45-, and 15-deg grazing angles appear in Figures 1, 2, and 13.

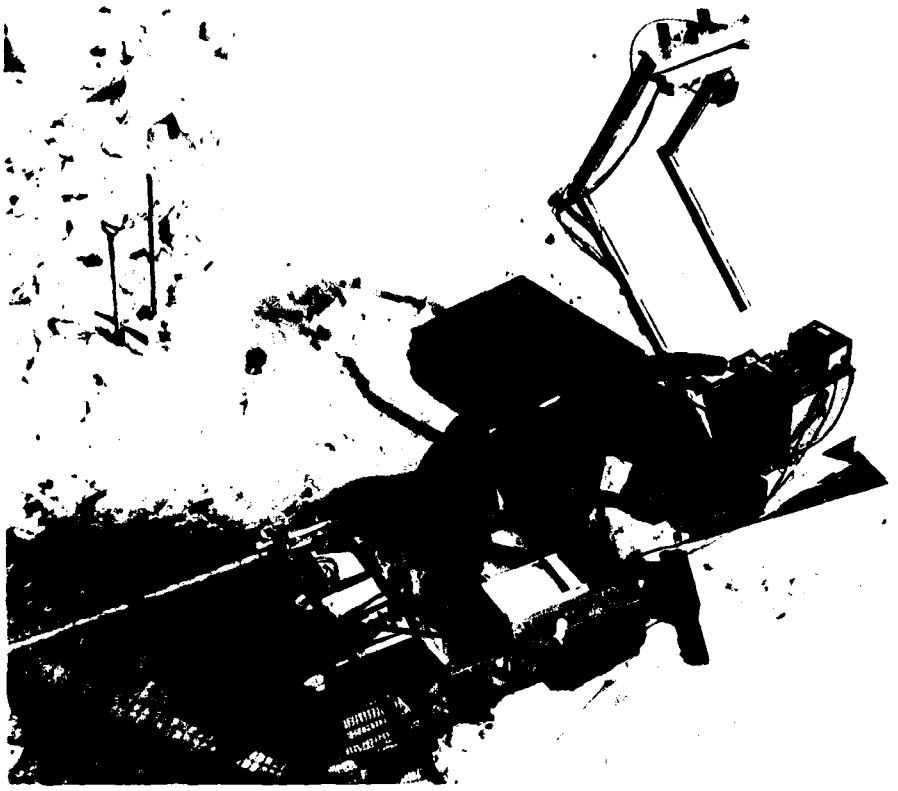

Figure 2. Snow Scatterometer, In-Situ Backscatter Mode (Positioned for 15-deg Grazing Angle Measurements)

The block diagram, Figure 3, illustrates scatterometer components and operation. In brief, the transmitters consist of 1-kHz squarewave modulated oscillators connected to standard-gain horn antennas. A Gunn oscillator generates the 35.1-GHz signal, and klystrons generate the 98.1- and 140.1-GHz signals. Standard-gain horn antennas also serve for reception. The receiver uses a single-ended Ka-band waveguide mixer. The Gunn local oscillator is tuned to obtain fundamental mixing at 35 GHz, third-order harmonic mixing at 98 GHz, and fourth-order har-

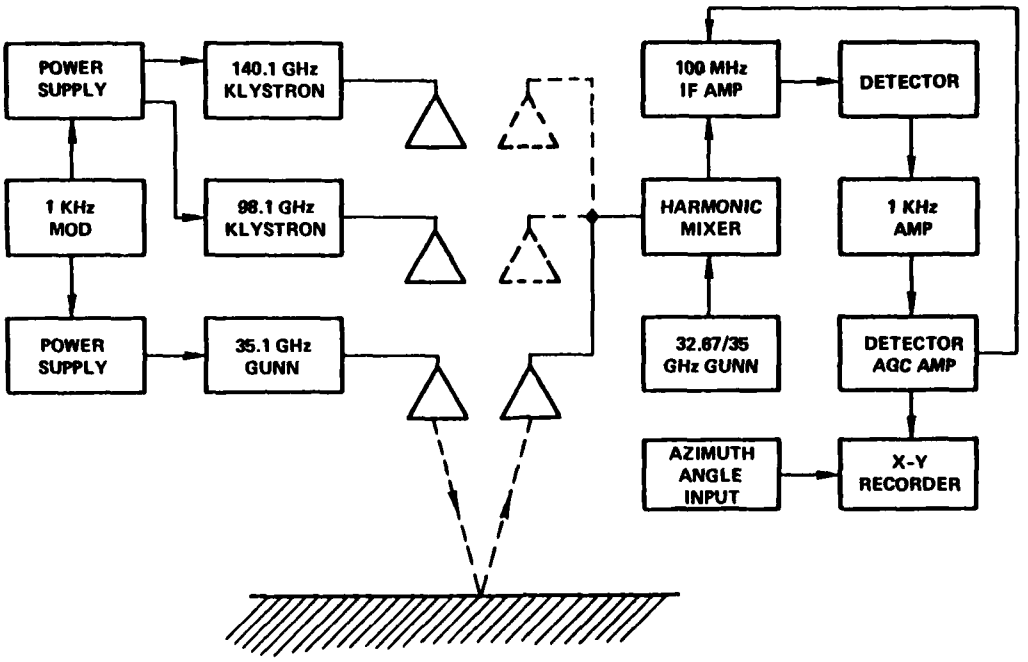

Figure 3. Scatterometer Block Diagram

monic mixing at 140 GHz. The resulting 100-MHz IF signal is amplified and detected. Narrowband post-detection amplification at 1 kHz is performed before the signal is recorded on the Y-axis of an XY-recorder. A voltage proportional to the angular position of the turntable is fed to the recorder X-axis. The snow-slab report[8] contains a more detailed description.

2.2 Measurement Procedures and Locations

A total of 240 in-situ snow scans were made over the period from 10 March to 20 March 1978. A scan produced data at fixed frequency, polarization, and grazing angle while rotating the scatterometer in azimuth through an arc of 270 deg. Scans were made at each of the three frequencies, at grazing angles of 90, 45, and 15 deg, and at vertical, horizontal, and crossed polarization.

In-situ measurements were carried out mostly during a period of cold nights and warm days. Under these conditions, snow ages through the so called melt-freeze (MF) process.[8] A day's measurements began at least 2 hours before sunrise to obtain a complete set of scans while the snow was still completely frozen. Immediately after that, a second identical set was begun. During this time, free water appeared as a result of solar heating. When the free-water content of the

snow was changing rapidly, horizontally polarized measurements were dropped at times to speed up the data collection. In one instance, measurements were made at only one frequency, 98 GHz.

As in the slab mode, the power ratio was measured between the returns from snow and from a large plane metal calibration plate. Figure 4 illustrates how

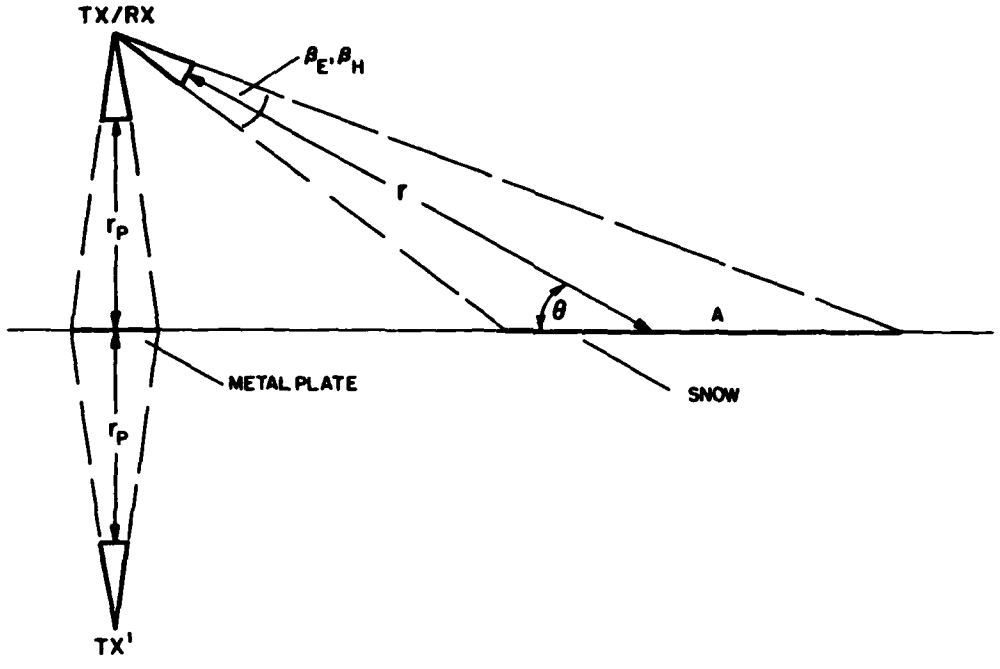

Figure 4. Image Source Calibration Procedure

the backscatter coefficient σ° per unit area snow can be determined. The power received from snow is calculated from the standard radar equation

$$P_R = \frac{P_T G_T \sigma^\circ A A_E}{(4\pi r^2)^2} \qquad (1)$$

with P_R received power
P_T transmitted power
G_T transmit antenna gain
A_E effective area of receiving antenna
r distance from transmitter/ receiver to snow
A snow area within 3-dB points of transmitted beam.

To a good approximation,

$$A = \frac{\pi \beta_E \beta_H r^2}{4 \sin \theta} \tag{2}$$

where β_E and β_H are the E- and H-plane 3-dB beamwidths, and θ is the grazing angle.

At perpendicular incidence (see Figure 4), image theory yields for the power received from the metal calibration plate at range r_p

$$P_{RP} = \frac{P_T G_T A_E}{4 \pi (2r_p)^2}. \tag{3}$$

Combining Eqs. (1), (2), and (3) and solving for σ° gives

$$\sigma^\circ = \frac{P_R}{P_{RP}} \cdot \frac{4 \sin \theta}{\beta_E \beta_H} \left(\frac{r}{r_p}\right)^2 . \tag{4}$$

Thus, σ° is calculated from the measured quantity P_R/P_{RP} and a number of known geometric parameters: the grazing angle, the transmit antenna beamwidths, and the range ratio.

At θ = 90 deg (Figure 1), the antennas passed over the metal plate during the first 40 deg of their 270-deg azimuthal scan. The antenna heights above the snow and the metal plate were identical in this case, $r_{90} = r_p = 2.13$ m. The scatter area moved along an arc of length s = 8.8 m during the 270-deg scan. The signal from the metal plate was checked at the beginning and at the end of a scan, and the chart recorder output was calibrated in dB below the metal plate signal, with a precision attenuator inserted after the first IF amplifier. At θ = 45 deg, the slant range to the snow was $r_{45} = 3.45$ m, and s = 16.8 m was traversed on the ground. The corresponding numbers for θ = 15 deg are $r_{15} = 9.14$ m and s = 43.4 m. All like- and cross-polarized measurements on snow were referenced to the perpendicular return from the metal plate.

The test area was an unobstructed, untraveled, essentially flat snow field of 120 by 190 m at Hanscom Air Force Base, 66 m above sea level. The site provided limited shelter for supporting functions and equipment storage plus access to line power. The scatterometer was set up new each day on a pedestal of packed snow in view of adjacent areas of virgin snow. The turntable and calibration plate were carefully leveled (Figure 1).

3. GROUND TRUTH MEASUREMENTS

During the in-situ tests, the following snow properties were monitored on a daily basis:

(1) Depth
(2) Density
(3) Hardness
(4) Temperature
(5) Stratigraphy
(6) Microstructure
(7) Surface Characteristics
(8) Free-Water Content

The majority of these parameters were determined with the Snow Observation Kit developed by the US Army Cold Regions Research and Engineering Laboratory (CRREL) and manufactured by Geotest Instrument Corporation, Wheeling, Illinois. The snow was characterized each day before the electromagnetic measurements began. A trench, as in Figure 5, was established in an area of unperturbed snow

Figure 5. Snow Trench Showing Collection of Ground Truth Data

near the backscatter area. The properties of a cross-section of snow at the end of the trench were recorded. Each day, the trench was extended to expose fresh snow. Except for temperature and free-water content, the snow parameters were not remeasured during the daily test period. Air and snow temperatures were taken during each scan. The free-water content was measured at least once every hour and sometimes twice every hour. A weather diary was maintained every day, regardless of the test schedule, to record noteworthy changes in weather conditions.

3.1 Measurement Techniques

Snow parameters (1) through (7) listed in Section 3 were measured in the same way as described in the snow-slab report.[8] Free-water content was determined only in connection with the in-situ program. Several different instruments are currently in use, and are, apparently, capable of measuring this parameter with sufficient accuracy. We used a melting-water calorimeter. Energy is conserved in a closed thermodynamic system undergoing physical changes such as melting. The expression for the initial energy content E_i (calorimeter partially filled with wet snow) is

$$E_i = C_p^w M_w T_w + C_p^i M_s^i T_s + H_f M_s^w + C_p^d M_d T_d. \tag{5}$$

After hot water has been added to melt the snow, the final energy content E_f becomes

$$E_f = C_p^w (M_w + M_s) T_e + H_f M_s + C_p^d M_d T_e. \tag{6}$$

The symbols in Eqs. (5) and (6) represent

C_p^d composite specific heat of dewar
C_p^i specific heat of ice
C_p^w specific heat of water
H_f heat of fusion of water
M_d mass of dewar
M_s^i mass of snow in the form of ice
M_s^w mass of free water contained in snow
M_s sum of M_s^i and M_s^w
M_w mass of hot water to melt snow
T_d initial temperature of dewar
T_e final equilibrium temperature
T_s initial temperature of snow
T_w temperature of hot water used to melt snow

Equating E_i to E_f and solving for M_s^i (the mass of the frozen part of the snow), one obtains

$$M_s^i = \frac{C_p^w M_w (T_w - T_e) - C_p^w M_s T_e + C_p^d M_d (T_d - T_e)}{H_f - C_p^i T_s} . \tag{7}$$

The last term in the numerator accounts for heat lost to the container.

The quantity $C_p^d M_d$ was determined in the following manner: The calorimeter (a 4-liter glass dewar) was brought to equilibrium with the outdoor temperature. A quantity of water at room temperature was filled in, and the dewar was agitated until it and the water reached equilibrium temperature. Omitting the snow terms in Eqs. (5) and (6) and solving for $C_p^d M_d$, we find

$$C_p^d M_d = \frac{C_p^w M_w (T_w - T_e)}{T_e - T_d} . \tag{8}$$

Measured results averaged at $C_p^d M_d = 93$ cal/1° C.

Relatively large quantities of snow (700 g) were used to determine its free-water content. With just enough hot water (98° C) to melt the snow completely but not to raise the final equilibrium temperature much above 0° C, the heat-loss term in Eq. (7) was kept small. During the experiment, the wide-mouthed dewar was covered with a 2-in. cork plate. No discernible heat loss by this route could be detected. No discernible heat loss resulted from the process of pouring hot water into the dewar. The overall accuracy of measured free-water content is estimated to be within 2 percent.

3.2 Snow Conditions During Tests

In-situ backscatter measurements were made on the six days from 10 March to 20 March 1978. During this period, snow conditions varied substantially. On 10 March, the top layer consisted of crusty snow that had been deposited on 4 March. Under this was a wide layer of loose snow from the big storm of 6 February.[8] The bottom layer was made up of ice, the remnant of a 20 January storm. The surface was highly irregular because of wind erosion (Figure 6).

Conditions producing strong MF metamorphism remained through 14 March. In the late afternoon of this day, rain began to fall. The rain, heavy at times, ceased in the evening. The night of 14-15 March was not cold enough for the wet snow to refreeze. Only late on 16 March did the temperature drop, and snow

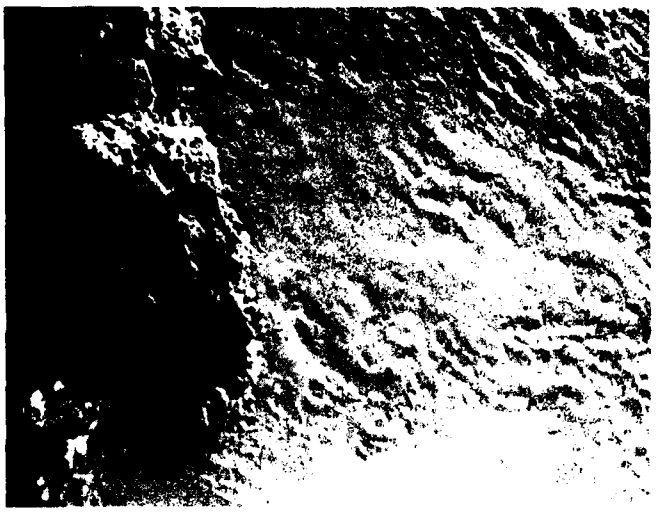

Figure 6. View of Snow Surface on 11 March 1978

began to fall. On 18 March, tests were conducted over approximately 15 cm of light, dry, powdery snow that lay on top of older snow and ice. The surface was relatively smooth (Figure 7). The next day, 19 March, was warm and sunny. It

Figure 7. View of Snow Surface on 18 March 1978

was followed by a cold night that turned the top snow cover into a crusty layer of MF snow. The surface took on a potholed appearance (Figure 8). A close-up photograph of the MF grains contained in this snow is shown as Figure 9. The small background raster is 1 by 1 mm.

Ground truth data are compiled in the Appendix for every day on which scatter measurements took place. Reference will be made to these data (Tables A1-A9) when discussing the backscatter results in the following sections.

Figure 8. View of Snow Surface on 20 March 1978

Figure 9. Close-up View of Larger Snow Grains of 20 March 1978 Shown on Millimeter Grid

4. DATA ANALYSIS

Typical raw-data plots recorded during the backscatter tests are shown in Figures 10-12 for 35, 98, and 140 GHz, respectively. The plots were obtained with the scatterometer set at a grazing angle of 90 deg and operating at vertical polarization. The abscissa in these figures represents the azimuthal position of the turntable with zero degrees set at some arbitrary position beyond the calibration plate. The ordinate is marked in signal level in decibel below that received from the calibration plate. The calibration signal is seen on the left side of each plot. Its "flat top" characteristic confirms that the antenna-footprint width along the direction of scan is substantially narrower than the width of the metal plate. The irregularity of the flat top is attributed to edge effects and the limited smoothness of the plate.

At about 40 deg from the beginning of the sweep, the antenna beams leave the calibration plate, and the fluctuating return from the snow is recorded over the remaining 230 deg of scan angle. Signals in Figures 10-12 are similar in appearance to those resulting from backscatter from snow slabs[8]. The strong fluctuations are caused by the random distribution of a large number of discrete scatterers, the snow granules. Their individual contributions to the sum signal, received by the scatterometer antennas, exhibit random phase that changes rapidly as the antennas sweep across the snow surface.

The 240 plots were analyzed to determine mean values of the backscatter coefficient and other statistical parameters. The fluctuation rate was measured as a function of signal frequency and grazing angle, and compared with a simple model of the scattering process.

4.1 Signal Fluctuation Rates

During the slab measurements, the scatterometer antenna beams pointed at a fixed location on the snow surface that rotated around an axis perpendicular to the beam direction. In order to obtain the approximate number of fluctuations per degree of slab rotation, the phasing between a stationary scatterer at the axis of rotation and one illuminated at the 3-dB point of the beam pattern was analyzed. The majority of scafterers are closer to the axis of rotation than to the edge of the beam. Also, the product of transmit and receive antenna beam patterns weights the contributions of the close-in scatterers more heavily than the contributions of those near the beam edge. This was qualitatively accounted for by analyzing phase changes between beam edge and beam center rather than between opposite beam edges. The latter would have increased the rate of change by a factor 2.

In the in-situ case, we apply the same rationale while adapting the equations to the geometry at hand. Figure 13 shows the scatterometer boom configurations

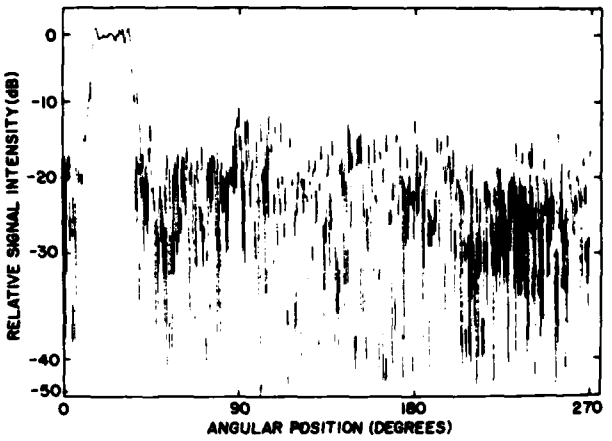

Figure 10. Snow Backscatter Intensity (Raw Data of 18 March 1978, 35 GHz, Vertical Polarization, 90-deg Grazing Angle)

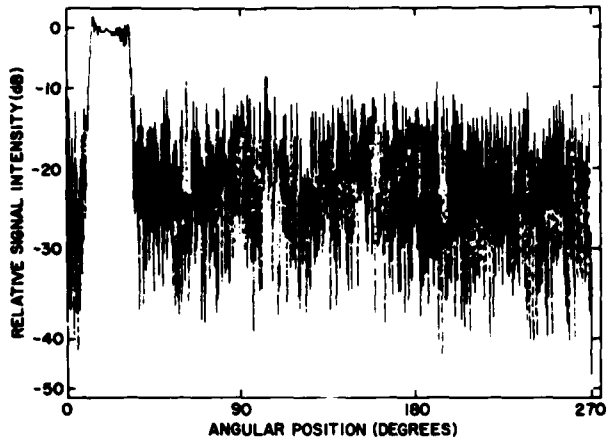

Figure 11. Snow Backscatter Intensity (Raw Data of 18 March 1978, 98 GHz, Vertical Polarization, 90-deg Grazing Angle)

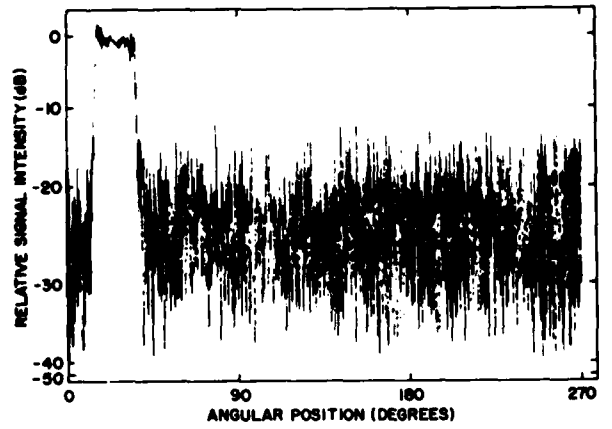

Figure 12. Snow Backscatter Intensity (Raw Data of 18 March 1978, 140 GHz, Vertical Polarization, 90-deg Grazing Angle)

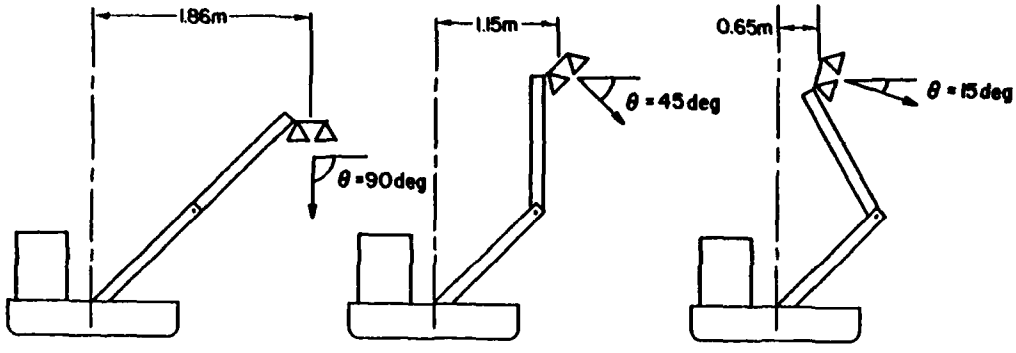

Figure 13. Scatterometer Positioned at Three Different Grazing Angles

for measurement at θ = 90, 45, and 15 deg. The dashed vertical line represents the axis of rotation. The center of gravity of the sled structure stays near the center of the turntable as the boom's upper portion is folded back to achieve the 45- and the 15-deg look angles. This leads to both a change in turning radius of the antennas and a change in height above the snow surface. Experimentally, the procedure is the most convenient one to change grazing angles, given the mechanical layout of the scatterometer.

While transmit and receive horns are actually mounted side by side, for purposes of determining the fluctuation rate, they are assumed to be co-located. Figure 14 shows the scatterometer antenna looking down at the snow in the 90-deg orientation. Scatterers S_1 and S_2 are located at the edge and at the center, respectively, of the antenna footprint on the snow surface. As the scatterometer antenna moves from position 1 to position 2 (distance d), it is implied that the signal scattered from S_2 undergoes no phase change. We derive the phase increase experienced by the signal scattered from S_1. The following equations are obvious by inspecting Figure 14:

$$d = r_o \sin \alpha \tag{9}$$

$$\ell_1^2 = \ell^2 + d^2 - 2\,\ell\, d \cos(\beta/2 + \pi/2). \tag{10}$$

For a small antenna displacement relative to scatterer range, $\ell >> d$, we substitute Eq. (9) into (10) and use a series approximation for Eq. (10),

$$\ell_1 = \ell + r_o \sin\alpha \sin(\beta/2). \tag{11}$$

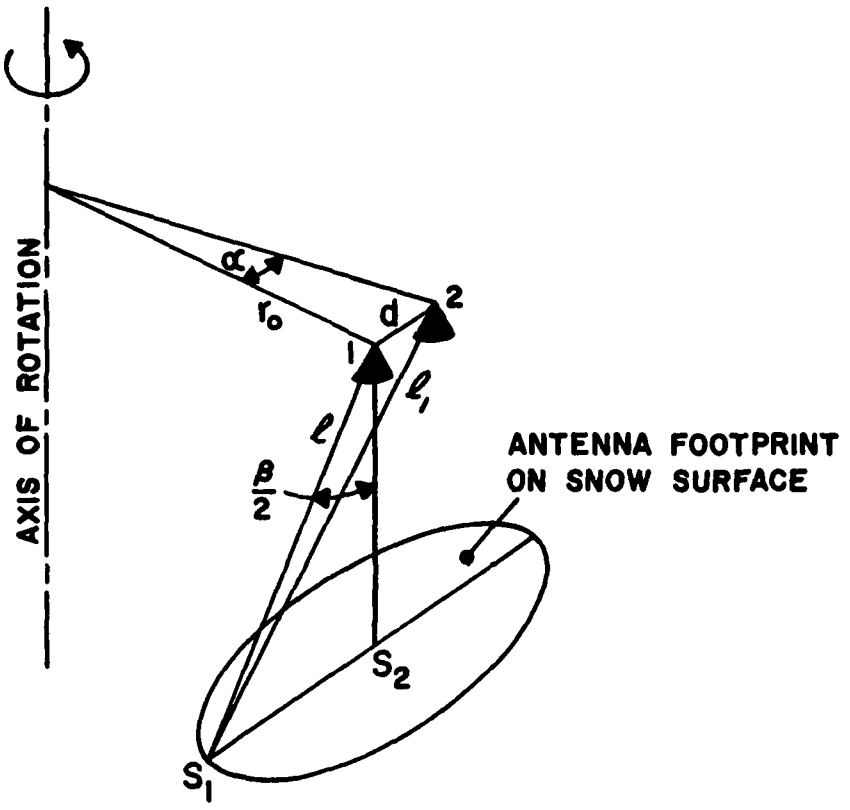

Figure 14. Antenna Scanning Geometry

The rate of range change with scatterometer rotation around the vertical axis then becomes

$$d\ell_1/d\alpha = r_o \cos\alpha \sin(\beta/2). \tag{12}$$

In the radar case, the range change doubles, resulting in a number of signal fluctuations per incremental angle $d\alpha$

$$d(2\ell_1)/\lambda = 2r_o \cos\alpha \sin(\beta/2)/\lambda \, d\alpha . \tag{13}$$

With the assumption of small angles α and β, we can write

$$d(2\ell_1)/\lambda = r_o \beta/\lambda \, d\alpha . \tag{14}$$

This result is similar to the one derived by Marshall and Hitchfield[9] for the condition of statistically independent sampling of the radar return from an array of scatterers randomly arranged in space. Decorrelation by their intuitive argument results when signals scattered from opposite edges of the beam change from originally equal and zero phase to values of $+\pi$ and $-\pi$ by lateral antenna motion over distance d. A more rigorous solution was published by Ruina,[10] who gives a comparable expression for the antenna displacement required to decrease the correlation between signals received to 1/e.

Signal fluctuation rates have been calculated from Eq. (14) for all wavelengths, scattering angles, and polarizations used in the experiment. Turning radii r_o are shown in Figure 13 for the three system orientations. Half-power beamwidths of the transmitting and receiving antennas are listed in Table 1. Note that the E plane

Table 1. E- and H-Plane Beamwidths of Transmitting and Receiving Antennas

Frequency (GHz)	Transmitting Antenna Calc. 3-dB Beamwidth		Receiving Antenna Calc. 3-dB Beamwidth	
	β_E(deg)	β_H(deg)	β_E(deg)	β_H(deg)
35	9.1	6.8	13.9	11.8
98	9.3	7.0	12.1	9.9
140	7.2	7.2	8.5	7.0

beamwidth determines the fluctuation rate for horizontal polarization. Correspondingly, the H-plane beamwidth is associated with the fluctuation rate of vertically polarized signals. Averages between transmit and receive beamwidths were used for the calculations. Results for vertical polarization are plotted as dashed lines in Figure 15. Also plotted in Figure 15 are averages of all vertically polarized measurements made over dry snow. The general slope of all curves, increasing fluctuation rate with increasing grazing angle, is mainly due to the r_o-change. The agreement between calculated and measurement values is reasonably

9. Marshall, J.S., and Hitschfeld, W. (1953) Interpretation of the Fluctuating Echo from Randomly Distributed Scatterers, Part I, Can. J. Phys. 31:962-94.

10. Ruina, J.P. (1963) The fluctuation of radar ground return due to antenna scanning, IEEE Trans. on Ant. and Prop. AP-11(No. 6):722-723.

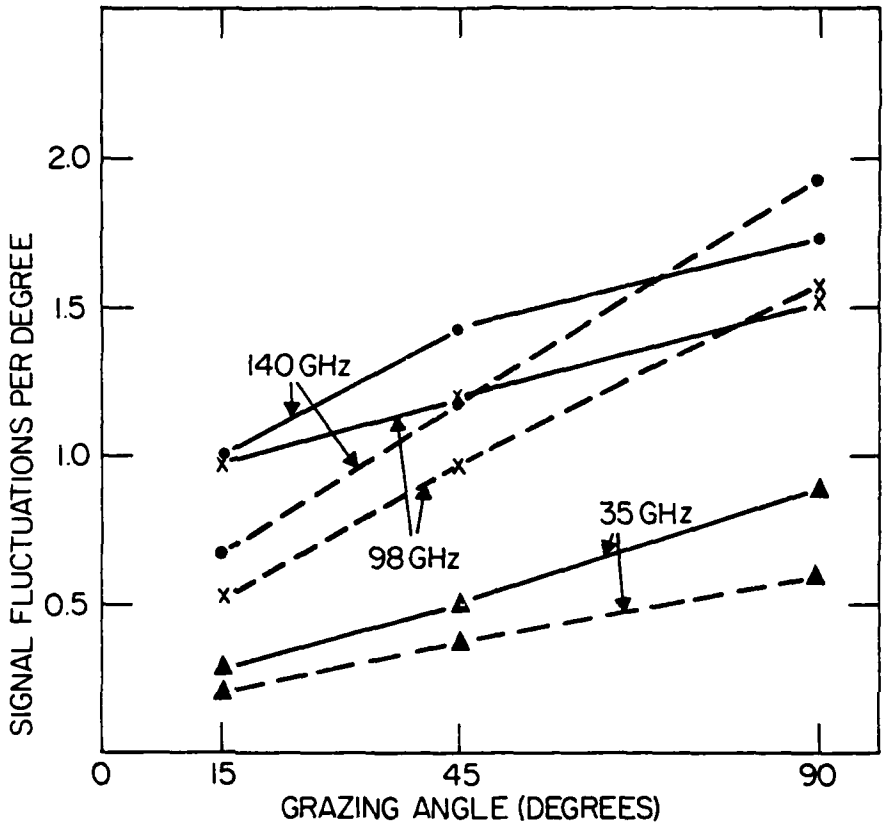

Figure 15. Backscatter Fluctuations (2π-phase Revolutions per Degree of Scatterometer Rotation) vs Grazing Angle (Measured —— and Calculated - - -, Vertical Polarization)

close. The deviations are not sufficiently systematic to attribute them, for example, to the simple assumption of phasing between beam-edge and beam-center signals. Subjective counting is likely to be a greater source of error. There is a tendency to undercount the higher fluctuation rates at the upper two frequencies. Results for horizontal polarization were similar and did not reflect the differences calculated in the E-and H-plane antenna beamwidths.

Data from snow cover containing meltwater showed a decrease in the observed fluctuation rate. A water film forming on the surface of the snow tends to smooth it. This causes a more specular return by increasing the reflected, nonfluctuating signal component arising near the location of S_2 (Figure 14). Scattered signal contributions from locations near S_1 suffer additional attenuation when passing obliquely

through the wet top layer of the snow.

4.2 Backscatter Statistics

Pen and ink plots of scattered signals created some problems in the data reduction process. At 35 GHz, extraction of mean value, standard deviation, and probability distribution of signal levels was readily accomplished. At 98 and 140 GHz, however, the scale of the X-axis (angular position) was too compressed in most cases to allow visual resolution of the signal structure other than the determination of the level of local maxima and minima. An examination of Figures 10, 11, and 12 proves this. Consequently, the mean, standard deviation, and probability distribution of signal peaks were determined at all frequencies.

At 35 GHz, where data could be analyzed completely, a relationship was established between the mean of the complete signal and the mean derived from the local peaks alone. It is assumed that this relationship holds at higher frequencies, where only local peaks are resolvable. Mean peak levels are determined by averaging over a large enough number n of local peaks (no more than 20) so that the average changes by less than 0.2 dB as n increases.

As an example, data gathered at 35 GHz on dry snow have been analyzed for a typical day (10 March 1978). Figures 16, 17, and 18 show the backscatter coefficient in decibel plotted on probability paper for vertical polarization and grazing angles of 90, 45, and 15 deg. Presented in this manner, lognormally distributed data fall on a straight line and Rayleigh-distributed data fall on a curved line of typical shape. In the figures, peak data match straight lines and complete data match Rayleigh curves well. The Rayleigh curves were fitted to pass through the median value of the measured σ°. Horizontal and crossed-polarization data resulted in similar plots.

The Rayleigh distribution of the complete signal is typical for a collection of randomly positioned scatterers, each contributing roughly equal power. The lognormal fit of the peak backscatter data was somewhat unexpected. However, Gumbel,[11] in his book on the statistics of extremes, states that the distribution of the extreme values of a statistic process quite often is of a lognormal nature.

For Rayleigh-distributed data, the relationship between the mean σ° and the median $\sigma^\circ_{0.5}$ of the backscatter coefficient is (in dB)

$$\sigma^\circ = \sigma^\circ_{0.5} + 1.6. \tag{15}$$

The cumulative probability curve does not change shape for different sets of data,

11. Gumbel, E. J. (1958) Statistics of Extremes, Columbia University Press, New York.

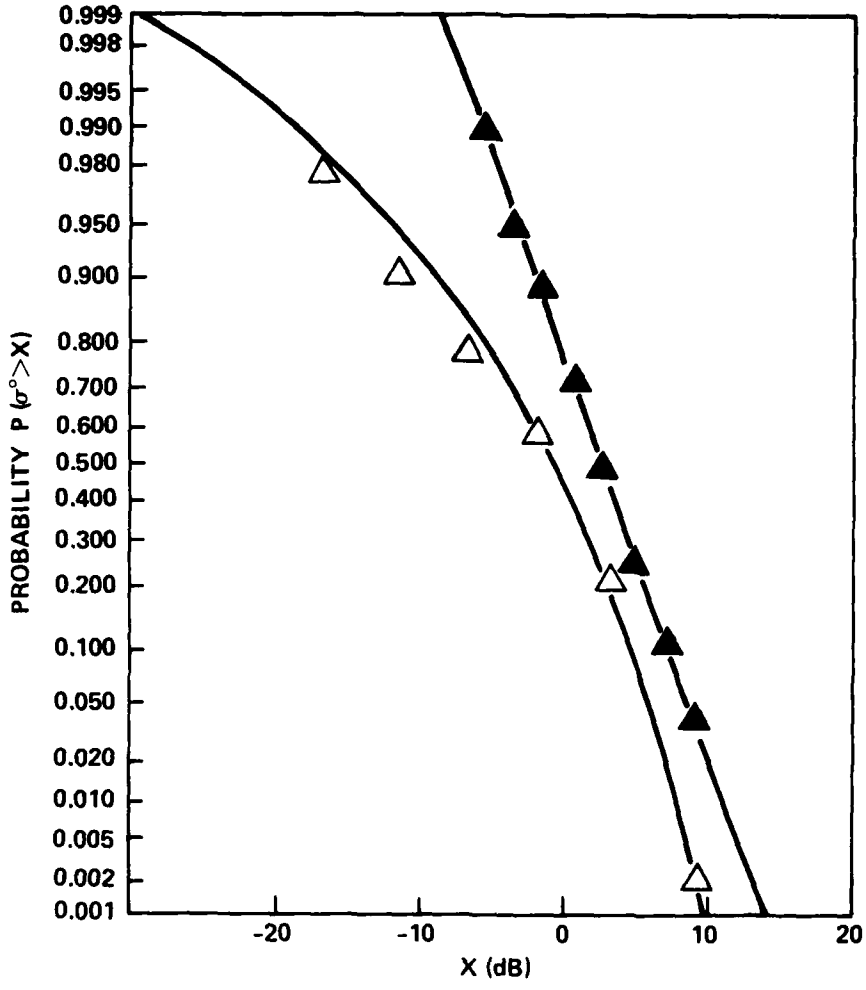

Figure 16. Cumulative Probability of σ° PEAK ▲——▲ and σ° △- - -△(10 March 1978, 35 GHz, Vertical Polarization, 90-deg Grazing Angle)

and the standard deviation S is a constant (2S = 11.3 dB). For lognormal data (in dB)

$$\sigma^\circ \text{ PEAK} = \sigma^\circ_{0.5} + 0.115\, S^2. \tag{16}$$

In this case, S is proportional to the slope of the straight line fitted to the data, and is explicitly given by one half of the distance on the abscissa between the cumulative

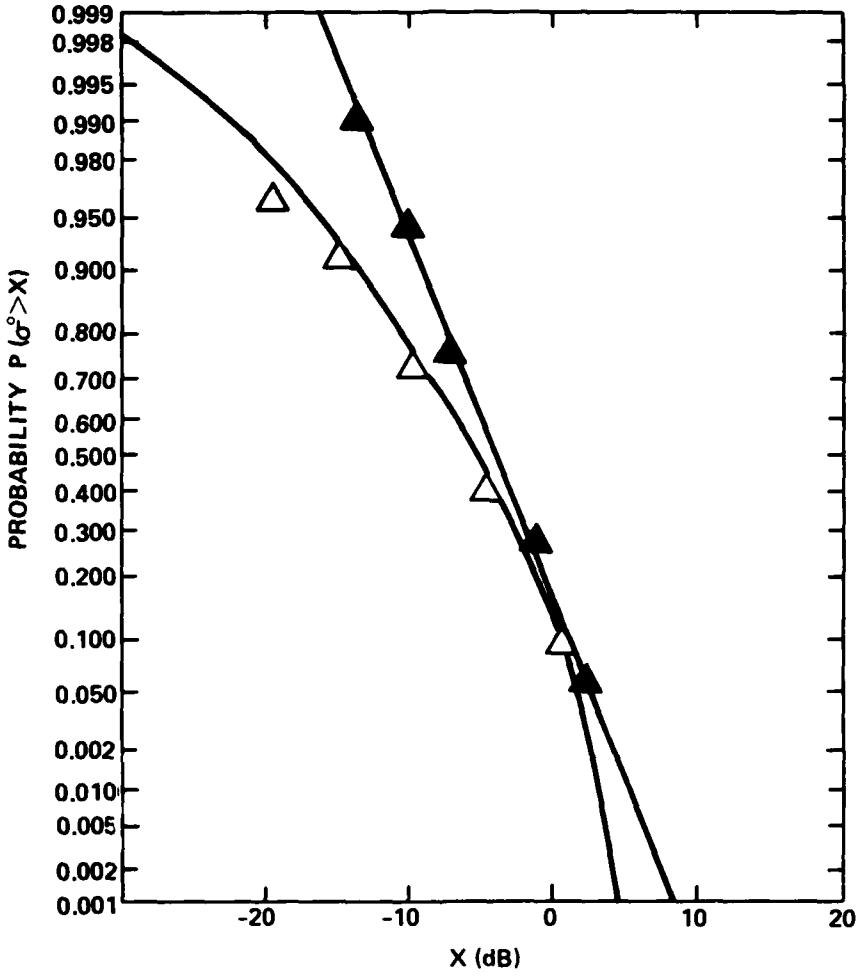

Figure 17. Cumulative Probability of σ°_{PEAK} ▲———▲ and σ° Δ- - -Δ (10 March 1978, 35 GHz, Vertical Polarization, 45-deg Grazing Angle)

probabilities of 0.84 and 0.16. Table 2 lists mean and mean-peak backscatter coefficients based on Eqs. (15) and (16) as well as the standard deviation of the peak backscatter coefficient. The differences between σ° and σ°_{PEAK} found on this particular day are compared to the averages of all 35-GHz measurements on frozen snow at vertical and horizontal polarization. The overall results show σ°_{PEAK} to exceed σ° by roughly 3 dB at 90-deg grazing angle, by 2 dB at 45-deg, and by 5 dB at 15-deg. As a firsthand approximation, we assume that the

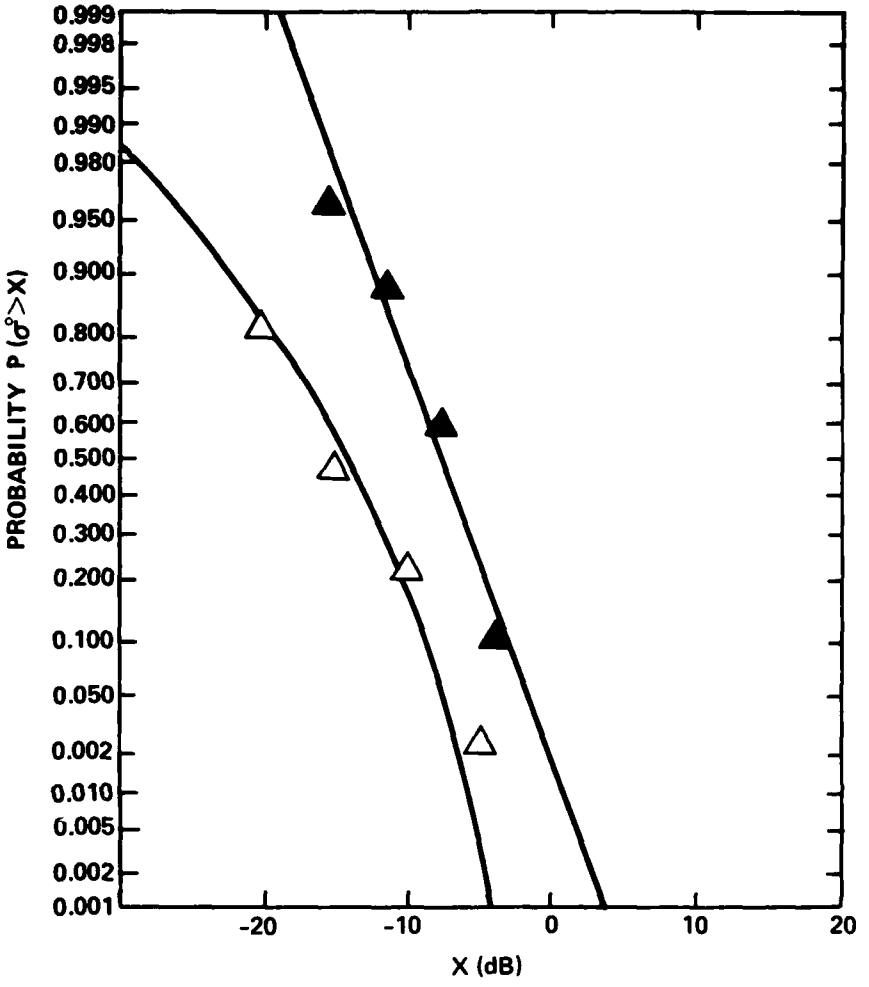

Figure 18. Cumulative Probability of $\sigma^{\circ}_{\text{PEAK}}$ ▲———▲ and σ° Δ - - - Δ (10 March 1978, 35 GHz, Vertical Polarization, 15-deg Grazing Angle)

mean-peak backscatter coefficient is 3 dB higher than the mean backscatter coefficient on average, and that we can extrapolate from this behavior at 35 GHz to 98 and 140 GHz.

In Figures 19 and 20, the cumulative probability distribution of $\sigma^{\circ}_{\text{PEAK}}$ is shown at 98 and 140 GHz for the same day. Again, a lognormal distribution is a good fit to all data taken over dry snow. The mean values and standard deviations for these cases are presented in Table 3. It is apparent from Tables 2 and 3 that the backscatter coefficient for dry snow increases with frequency and grazing

Table 2. Mean and Standard Deviation of Backscatter Coefficients for 35 GHz at T < 0° C

Grazing Angle (deg)	Mean Backscatter Coefficient		Standard Deviation of σ°_{PEAK} S (dB)
	σ° (dB)	σ°_{PEAK} (dB)	
90	0.5	4.0	3.4
45	-4.3	-2.1	4.3
15	-12.8	-6.4	3.5

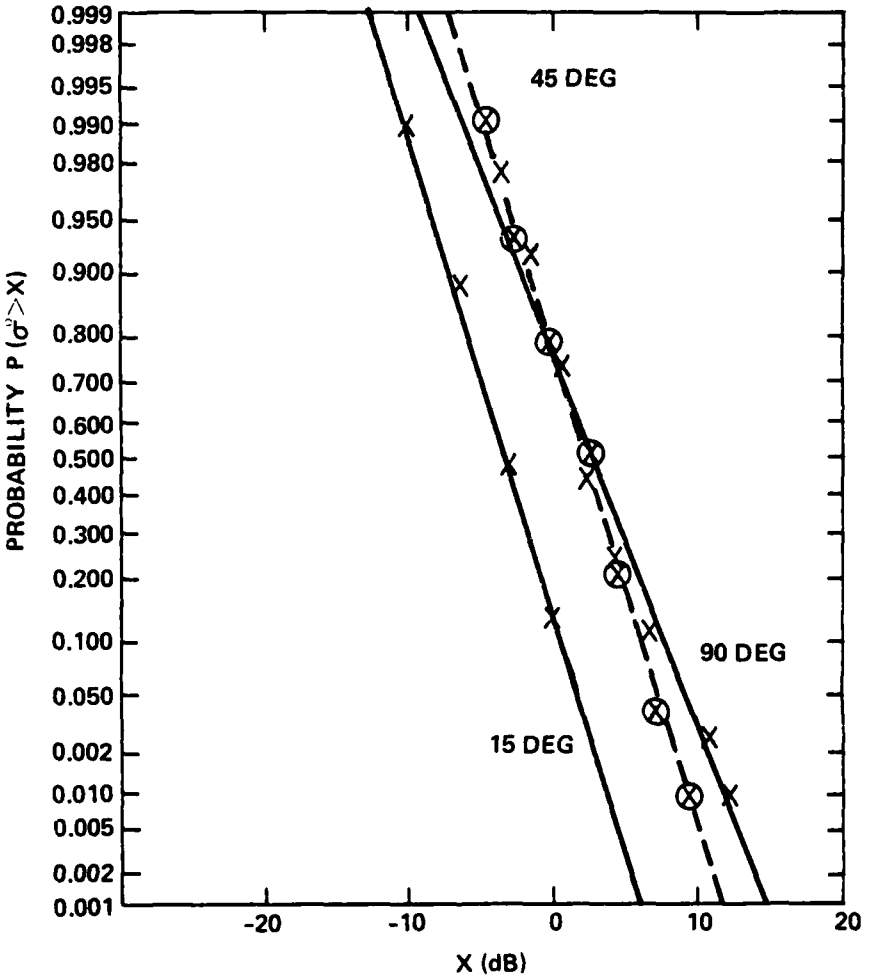

Figure 19. Cumulative Probability of σ°_{PEAK} (10 March 1978, 98 GHz, Vertical Polarization)

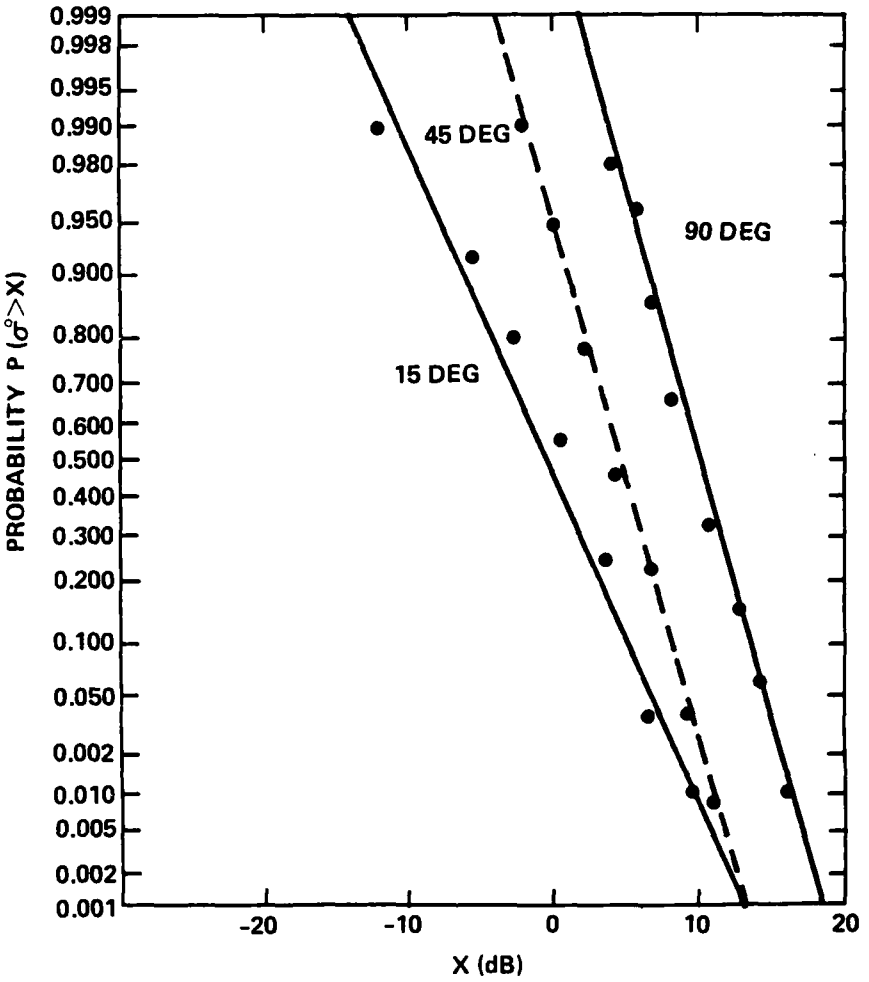

Figure 20. Cumulative Probability of σ°_{PEAK} (10 March 1978, 140 GHz, Vertical Polarization)

angle. This dependence will be looked at in greater detail in the next section.

The data discussed so far were collected at air temperatures of less than 0°C with no free water present. When the temperature rose above 0°C and melt-water appeared later during the day, the complete signal statistics at 35 GHz could be established only at perpendicular incidence. Although more spread occured in the σ°_{PEAK}-data points for $T > 0^{\circ}C$ than was the case for dry snow (Figure 18), a lognormal straight line still provided a reasonable fit to the data. However, a Rayleigh curve no longer matched the measured distribution of the complete signal.

Table 3. Mean and Standard Deviation of Peak Backscatter Coefficient for 98 and 140 GHz at T < 0°C

Grazing Angle (deg)	98 GHz		140 GHz	
	σ°_{PEAK} (dB)	S (dB)	σ°_{PEAK} (dB)	S (dB)
90	4.3	4.0	10.7	2.5
45	3.1	3.1	5.1	2.8
15	-2.5	3.0	2.5	4.7

Wet-snow σ°_{PEAK}-data of 10 March 1978 at the two lower grazing angles at 35 GHz, and at all grazing angles at 98 and 140 GHz, agreed fairly well with lognormal distributions, too. Table 4 contains σ°_{PEAK}-and S-values at the three frequencies and at perpendicular incidence for above-freezing snow. A drop in the mean-peak backscatter coefficient for wet snow is apparent at all frequencies (compare Tables 2, 3, and 4). Again, this will be discussed in greater detail in the next section.

Table 4. Mean and Standard Deviation of Peak Backscatter Coefficient for T > 0°C at 90-deg Grazing Angle

Frequency (GHz)	σ°_{PEAK} (dB)	S (dB)
35	0.9	5.6
98	2.9	5.0
140	6.3	2.7

4.3 Backscatter Coefficients

We consider only peak backscatter coefficients in the remainder of this report. Therefore, we no longer refer to the data as peak data nor designate the peak backscatter coefficient as σ°_{PEAK}. Unless stated otherwise, σ° will stand for mean-peak values in what follows. Vertical, horizontal, and cross-polarized backscatter

coefficients are distinguished by subscripts VV, HH, and HV. Here V and H represent vertical and horizontal, with the first letter denoting transmitted, and the second letter denoting received polarization. Backscatter coefficients will be presented in three different formats: (a) dry- and wet-snow data on individual days versus grazing angle; (b) averages of all data versus grazing angles; and (c) averages of all data versus frequency.

A nearly complete set of measurements on frozen and melting snow was obtained on two days, 10 and 18 March 1978. The snow cover was quite different on these two days. On 10 March, a crusty top layer had developed from snow deposited six days earlier. On 18 March, a 12- to 15-cm thick layer of new light snow covered the test area. The surface was quite rough on the earlier day, as demonstrated in Figure 6. It was relatively smooth on the latter day, as seen in Figure 7. The air temperature rose rapidly after sunrise on 18 March. Measurements in the horizontally polarized mode were, therefore, omitted over frozen snow to allow the more rapid collection of a data set. Once the air temperature exceeded 0°C, horizontal polarization was included.

Backscatter coefficients at 35 GHz are displayed in Figure 21 for 10 March and in Figure 22 for 18 March. The general variation is the same for corresponding curves in both figures. For dry snow, σ°_{VV} exceeds 0dB at 90 deg and is lower by 10 to 15dB at 15-deg grazing angle. The same trend holds true for σ°_{HH} (Figure 21), although the drop is more rapid as the grazing angle becomes smaller. Averaging all available 35-GHz data over dry in-situ snow suggests that there may be some significance to the more rapid drop-off, but not to the difference at perpendicular incidence. Cross-polarized backscatter coefficients behave like the vertically polarized ones, being between 5 and 10 dB less in both figures at each angle θ. Note the increasing rate of σ°-drop for dry snow as the grazing angle decreases (θ is plotted on a linear scale).

The opposite is true for the wet-snow data at this frequency. Free water produced a dramatic change in the angular dependence of σ°. While the backscatter coefficient is only moderately affected in the like-polarized case at θ = 90 deg, it drops at a much higher rate between 90 and 45 deg than previously seen for dry snow. Although the three-point representations of angular variation of σ° in the in-situ mode are crude, they do suggest a specular contribution to wet-snow scatter at this frequency, similar to that found on ice surfaces of frozen snow slabs.[8] This interpretation is supported by the substantial drop in σ°_{HV} approaching 20dB at perpendicular incidence.

An indication of a smoother snow surface on 18 March is seen in the σ°_{VV}- and σ°_{HH}-levels for wet snow at 90 deg. They are 5dB higher than those of 10 March. This is thought to be the effect of reflection from a smooth waterlogged layer near the surface of the snow. Despite the dissimilarity of the snow on both

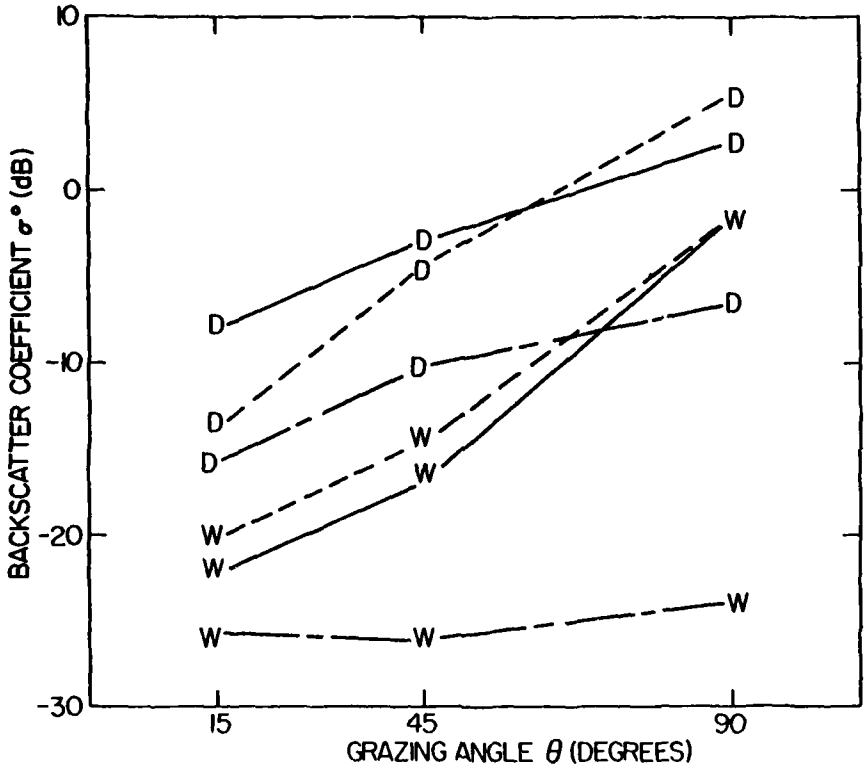

Figure 21. σ° vs Grazing Angle (10 March 1978, 35 GHz; Dry Snow, Polarization VV D—D, HH D- - -D, HV D-.-.-D; Wet Snow, Polarization VV W—W, HH W- - -W, HV W-.-.-W; Free-Water Content 4.7 Percent)

days (Tables A1 and A5), the results are surprisingly similar. We assume that, during the dry phase, the effect of the underlying packed snow is strongly seen. That is, the 35-GHz signal scattered from this type of snow is not attenuated much as it travels through the lighter snow on top. During the wet phase, snow parameters other than the liquid-water content apparently became less significant for the scatter process. Tables A7 and A9 reveal quite similar percentages of liquid water during the measurements in Figures 21 and 22.

The curves in Figure 23 are based on averages of all 35-GHz backscatter coefficients obtained from in-situ snow. The free-water content, on which the wet-snow data in this figure are based, ranges from a low of 3 percent to a high of 15 percent by weight. In view of the effect of the snow/water ratio on backscatter, this may look like an oversimplification. However, the smoothing of the data achieved in the process appears to benefit the comparison of all in-situ data later

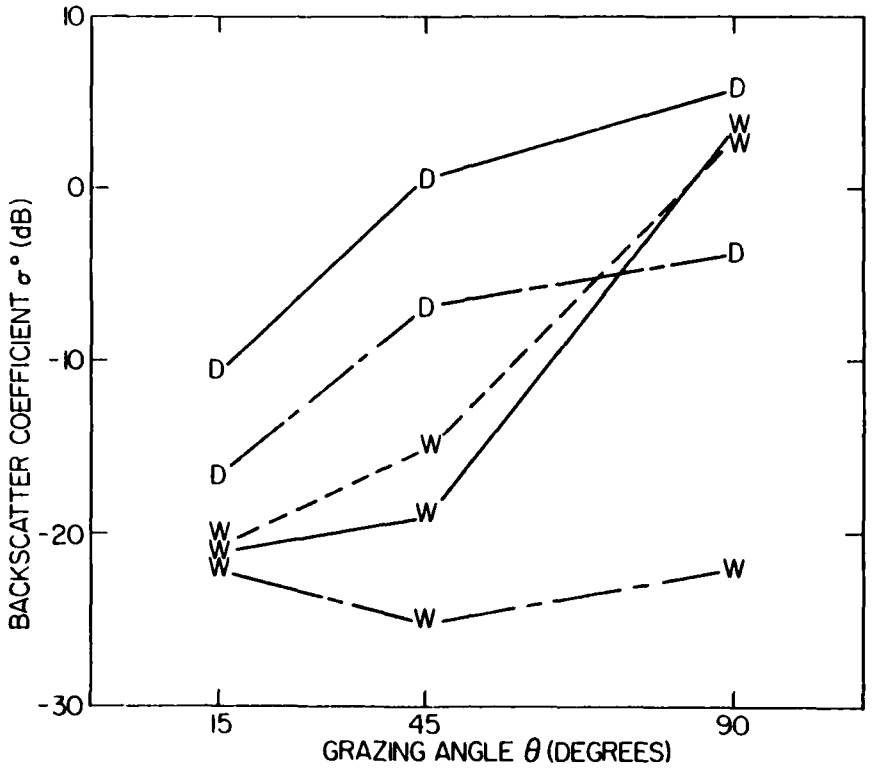

Figure 22. σ° vs Grazing Angle (18 March 1978, 35 GHz; Dry Snow, Polarization VV D—D, HH D- - -D, HV D-.-.-D; Wet Snow, Polarization VV W—W, HH W- - -W, HV W-.-.-W; Free-Water Content 4.8 to 5.3 Percent)

on. No great change occurs in the average 35-GHz curves relative to the ones already displayed for individual days. Corresponding like-polarized σ° are essentially equal. A reason for the slightly higher σ°_{HH} for wet snow and the slightly lower σ°_{HH} for dry snow is not apparent.

The specular behavior is well pronounced for the overall data. The relatively high return from wet snow at 15 deg and crossed polarization on 18 March does not prevail in the overall data.

At 98 GHz, the backscatter coefficient from dry and wet snow was measured on four days. On 11 March, having probed the dry snow at all frequencies, the decision was made to limit subsequent measurements to only one frequency, 98 GHz, and to observe the effect of changing free water on backscatter more continuously. The 98-GHz data of 10 March are shown in Figure 24. Dry-snow values for like polarization are higher by several dB at perpendicular incidence and conti-

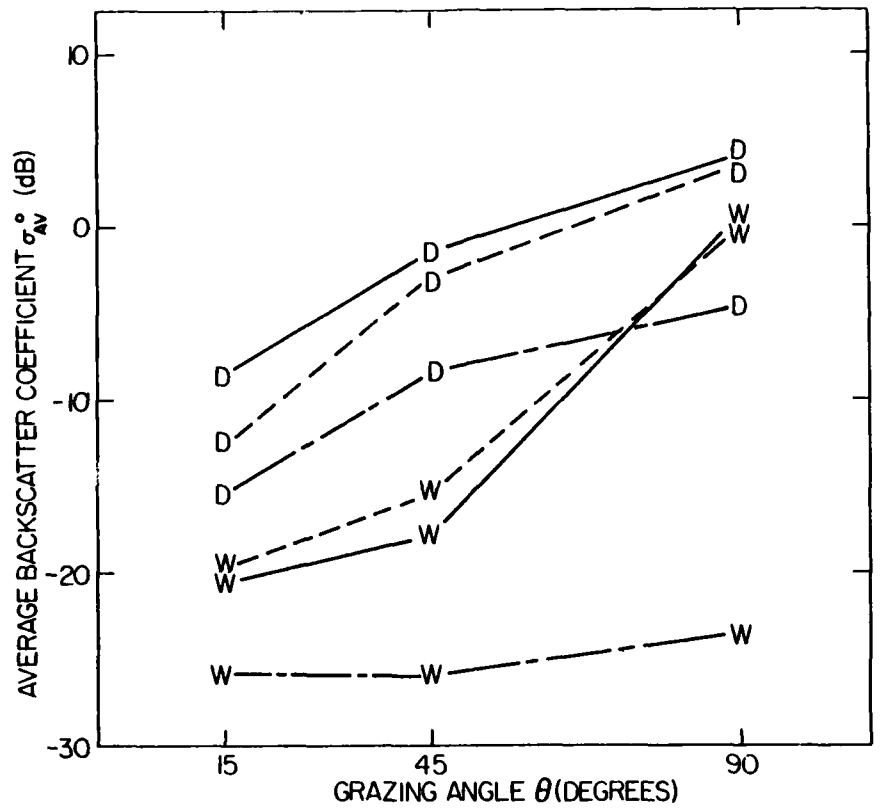

Figure 23. Average of σ° for All In-Situ Data (35 GHz; Dry Snow, Polarization VV D—D, HH D- - -D, HV D-.-.-D; Wet Snow, Polarization VV W—W, HH W- - -W, HV W-.-.-W; Free-Water Content 3 to 15 Percent)

nue to be higher at the lower angles in comparison with averages at 35 GHz. Again, the crossover is not considered to be significant. There is some indication that σ°_{HV} is larger relative to σ°_{VV} and σ°_{HH} at this frequency. This is particularly the case at 45 deg, and is also confirmed by the 98-GHz average curves.

Free water leads to several characteristic differences between the results at the lower two frequencies. In Figure 24, we do not see the steep drop in σ°_{VV} and σ°_{HH} (away from θ = 90 deg) that was typical of a specular scattering process. The specular contribution, if it exists, is hardly noticeable for vertical polarization. For horizontal polarization, the rate of σ°-drop resembles that of dry snow. That is, it increases with decreasing grazing angle. At 15 deg, σ°_{VV} of wet snow exceeds σ°_{HH} of dry snow. This fact would be questionable had it not

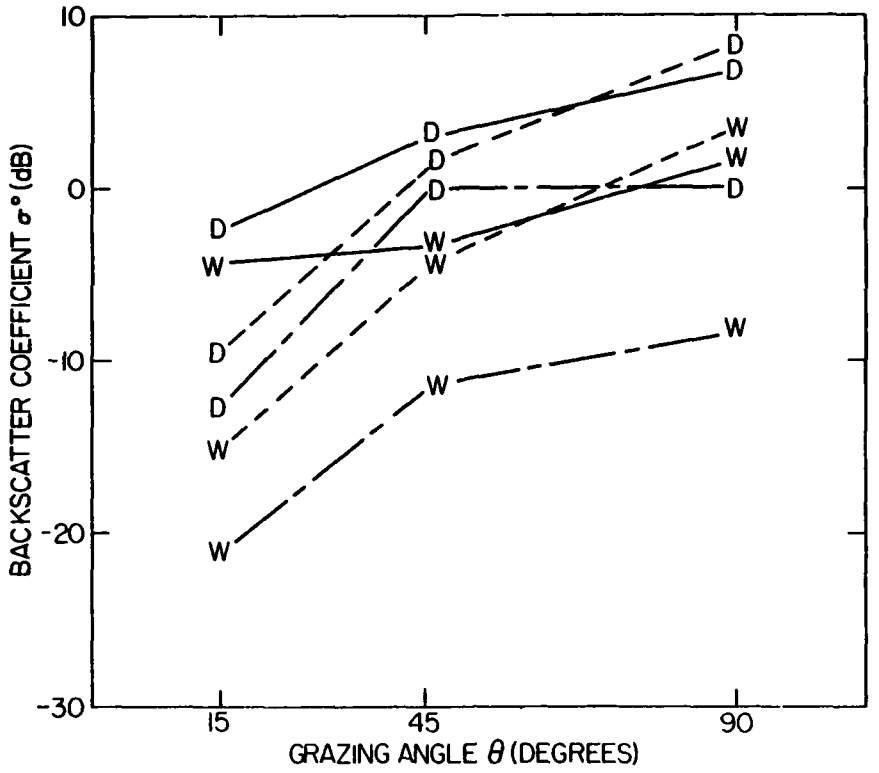

Figure 24. σ° vs Grazing Angle (10 March 1978, 98 GHz; Dry Snow, Polarization VV D—D, HH D- - -D, HV D-.-.-D; Wet Snow, Polarization VV W—W, HH W- - -W, HV W-.-.-W; Free-Water Content 5 Percent)

also been found on 18 March (Figure 25), the other day on which horizontally polarized measurements were performed.

In contrast to the 35-GHz findings, the cross-polarized component of the backscatter signal is reduced much less at 98 GHz when the snow contains meltwater Changes as large as 20dB were seen in Figures 21 and 22, but the maximum seen in Figures 24 and 25 is about 10dB. Actually, at 15 deg on the 18th of March, the reduction in cross-polarized backscatter coefficient is only 1 dB. The σ°_{HV}-curves for wet snow exhibit an angular dependence at 98 GHz similar to the majority of the other curves at this frequency. This is indicative of rough-surface or volume scatter and is in contrast with the specular appearance of the wet snow at 35 GHz.

The curves in Figure 26 represent averages of all data taken at 98 GHz over wet and dry snow. Again, as in Figure 23 for 35-GHz data, a wide range of free-

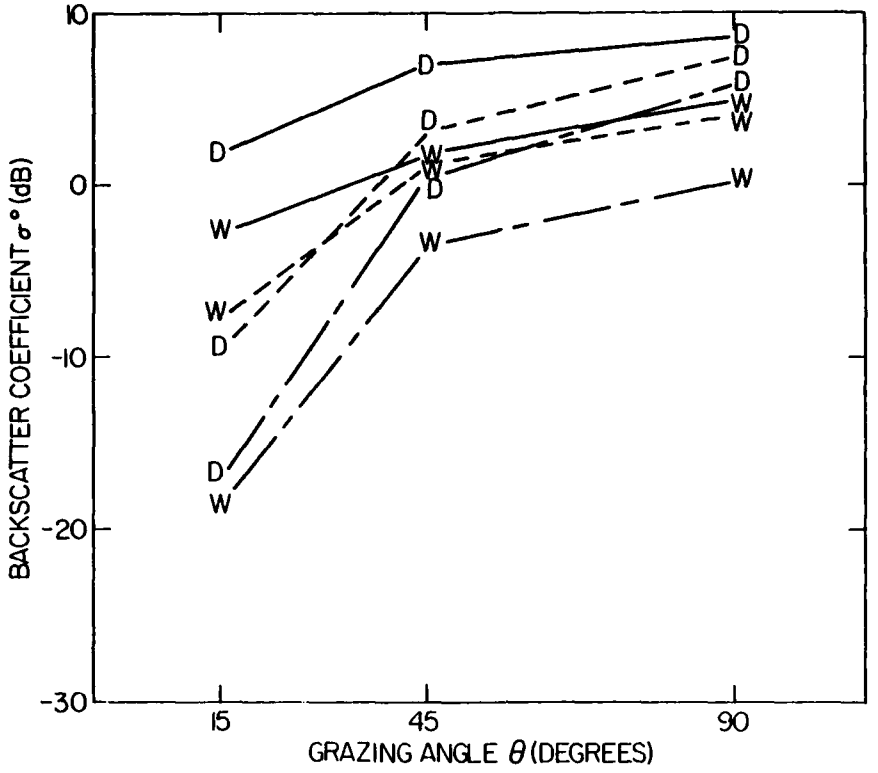

Figure 25. σ° vs Grazing Angle (18 March 1978, 98 GHz; Dry Snow, Polarization VV D—D, HH D- - -D, HV D-.-.-D; Wet Snow, Polarization VV W—W, HH W- - -W, HV W-.-.-W; Free-Water Content 7 to 9 percent)

water content (3-16 percent) contributed to the σ°-curves. This should be kept in mind as well as the fact that, for technical reasons, the substantial quantities of snow required could not be dug from a shallow layer. Therefore, the free-water content is averaged over the width from the surface to the depth specified in Tables A7 to A9. The depth of snow removal was chosen differently at times in order to assess vertical inhomogeneities in the water concentration. Discrepancies between snow sampling depth and millimeter-wave penetration depth may be significant, particularly at the higher two frequencies.

Visually, it is obvious that the average curves of σ° are less spread apart at 98 GHz and at higher levels than those at 35 GHz. For dry snow, σ°_{HV} approaches σ°_{VV} and σ°_{HH} more closely toward the 90-deg grazing angle than was found at the lower frequency. This is understandable since the nonspecular scatter process can provide a relatively stronger cross-polarized return. The

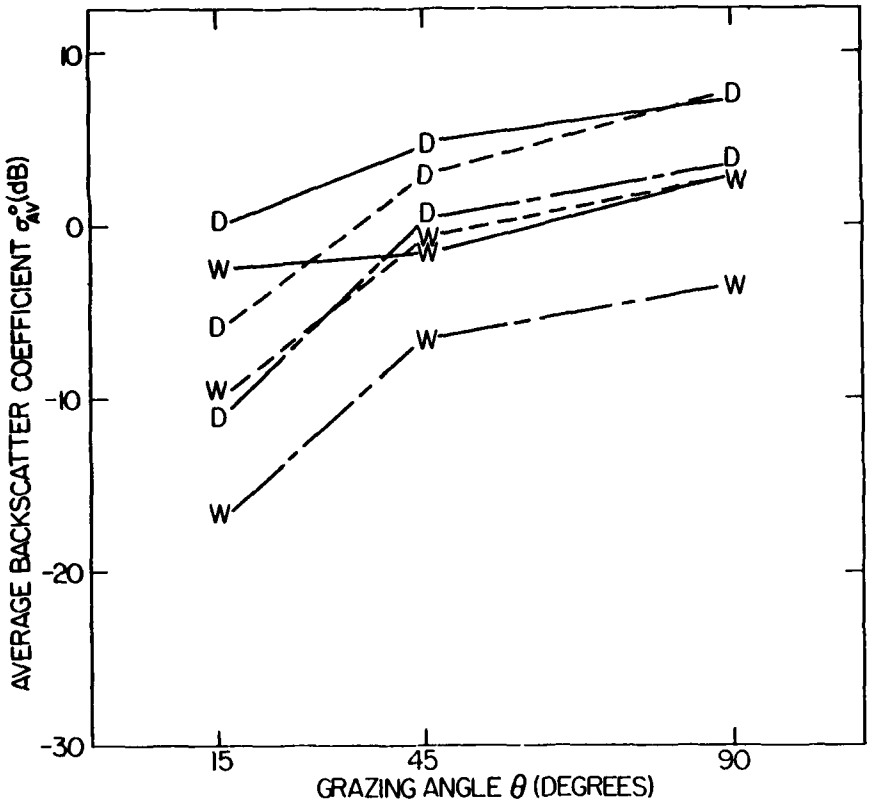

Figure 26. Average of σ° for All In-Situ Data (98 GHz; Dry Snow, Polarization VV D—D, HH D- - -D, HV D-.-.-D; Wet Snow, Polarization VV W—W, HH W- - -W, HV W-.-.-W; Free-Water Content 3 to 16 Percent)

wet-snow averages largely follow the grazing angle dependence already described for individual days. The segment of σ°_{VV} between 15 and 45 deg for melting snow still shows a slope resembling the corresponding 35-GHz curve (specular scatter). The comparatively wide spread and crossover of σ°_{VV} and σ°_{HH} at the lower θ remains somewhat disturbing. It does not show up at 140 GHz.

On 11 March, data collection at 98 GHz continued all day, as mentioned before. The diurnal variations for the VV-mode and the HV-mode are seen in Figures 27 and 28, respectively. In each figure, σ° is plotted as a function of time. Air temperature and time of sunrise (SR) and sunset (SS) are marked on the abscissa. The ordinates are scaled for backscatter coefficient and free-water content (FWC). The heavy dots on the lower curve represent measured percentages of liquid water.

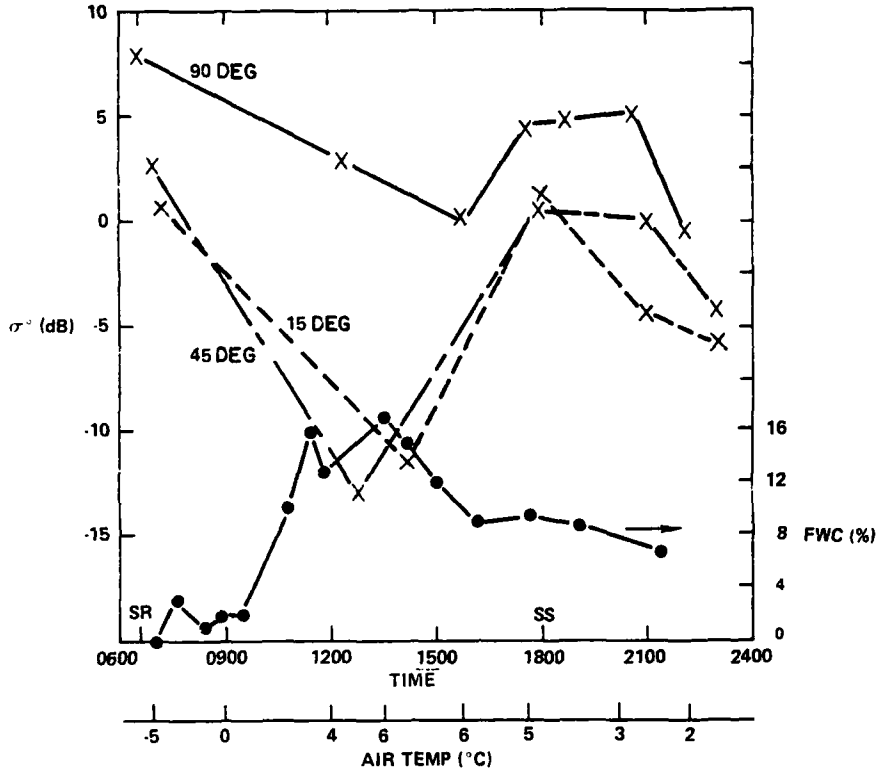

Figure 27. σ° and Free-Water Content (FWC) vs Time of Day (In-Situ Data of 11 March 1978, 98 GHz, Vertical Polarization)

The curves of free-water content are identical in both figures. The free-water content begins to rise appreciably shortly after 0900 and reaches a maximum in excess of 15 percent before noon. The high level of FWC is maintained to around 1400. From that time on, a steep drop occurs to around 9 percent, which is reached at about 1600. Beyond 1600 and until the end of the measurement at 2300, the free-water content diminishes at a slow rate. At 2125, 6.7 percent of free water was still found in the snow.

The period of heavy melting in the morning hours corresponds with a substantial reduction in σ°_{VV} and σ°_{HV} at all three scatter angles. The millimeter-wave data points during this period are too infrequent to establish an exact correspondence with the free-water curve. They do show that the lowest levels of like- and cross-polarized backscatter coincide with the period of highest free-water content between noon and 1500. An interesting phenomenon is seen in the later part of the day: the free-water content becomes less from 1330 on. It never

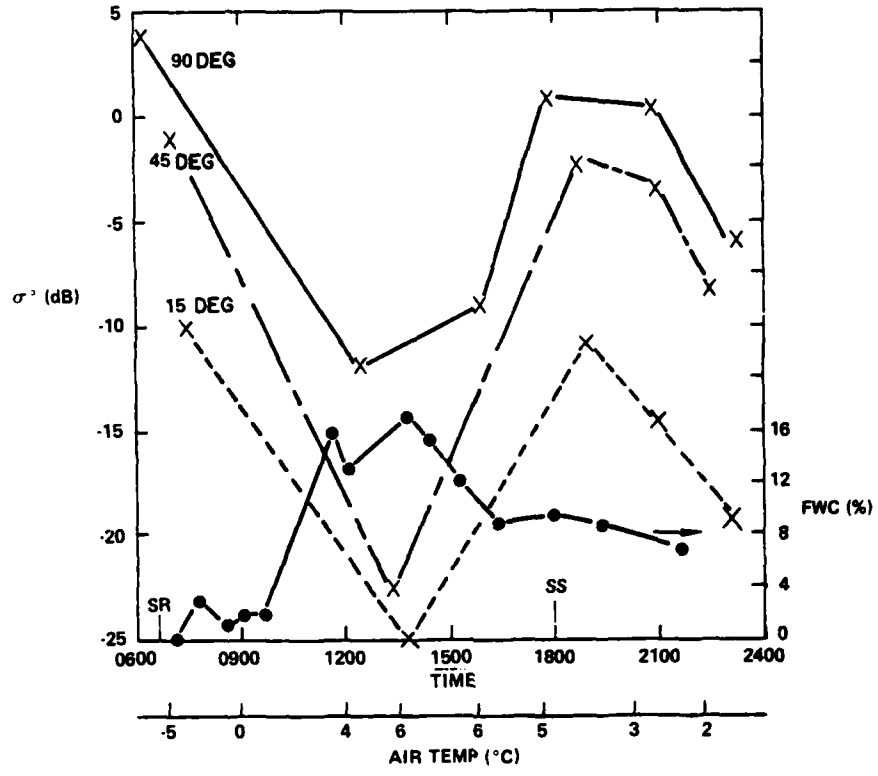

Figure 28. σ° and Free-Water Content (FWC) vs Time of Day (In-Situ Data of 11 March 1978, 98 GHz, Cross-Polarization)

drops to levels lower than 6.7 percent during the remainder of the measurements, which is still relatively high. One would not be surprised if the backscatter did not change much during this time. Other work[6] has demonstrated a large decrease in backscatter coefficient even when as little as 3 percent water remains in the snow. In contrast to this, the backscatter coefficients, both like- and cross-polarized, experience a substantial recovery during the early period of disapp- ing free water. The relatively high levels of σ°_{VV} and σ°_{HV} are sustained for several hours around sunset before they begin to drop again substantially, without any apparent clue from the free-water curve.

An explanation is possible for the signal recovery around 1500. As the snow melts near the surface, meltwater percolates down to the lower levels of the snow cover. Melting caused by solar heating increases before noon so that the rate of production of meltwater exceeds the rate of downward percolation. Consequently, the snow near the surface contains a higher percentage of meltwater than the snow

in the lower layers. As the solar radiation decreases later in the afternoon, the percolation rate at some point exceeds the rate of meltwater production. The free-water content near the surface decreases below the average free-water content sampled by our calorimetric technique. Judging from the attenuation coefficient measured on dry snow slabs at 98 GHz,[8] 2 to 4 dB/cm, which is low compared with the wet snow under investigation, the backscatter signal at this frequency may well have originated in the top 1 or 2 cm of the medium. Possibly, this pertains only to times of extremely strong melting, like 11 March. The millimeter-wave signal sensed snow dryer than it was on average.

Over the 3-hour period after sunset and beyond, free water continued to disappear from the snow layer under measurement. By 2300, it became clear that the air temperature would remain above 0°C throughout the night and that it would not be possible to monitor the refreezing process. We decided at this time to terminate the experiment. Using hindsight, we realize that data collection should have continued until later in the night to shed light on the σ°_{VV}- and σ°_{HV}-drop later during the evening. The renewed fall-off of the backscatter coefficient at both polarizations and at all grazing angles implies an increase in water concentration near the surface. This cannot easily be explained, since the sun is down and the air temperature is falling (Figure 28).

The data in Figures 27 and 28 are the result of a single day's measurements. Comparison with the 98-GHz averages in Figure 26 shows that, for dry snow, σ°_{VV} and σ°_{HV} agree within 2 dB at all grazing angles. The same is true for σ°_{VV} at perpendicular incidence throughout the melting phase. At θ = 45 and 15 deg, σ°_{VV} and σ°_{HV} are lower than the average data by about 10 dB during the very wet period in the morning. They are within 2 to 3 dB from midafternoon on. The cross-polarized σ° at all grazing angles show declines during the wettest period to values about 10 to 15 dB lower than the ones in Figure 26. Again, from midafternoon on, levels move into the range shown by the average data.

The relatively normal behavior of σ°_{VV} at θ = 90 deg and the abnormally low σ°_{VV} and σ°_{HV} in all other cases suggest a specular reflection on the wet snow. To the extent that the water in the top layer appears like a plane, lossy dielectric layer to the millimeter-wave signal, no return is expected for like polarization at the lower grazing angles. No cross-polarized return is expected at any grazing angle. Whether or not this condition was met by the snow shown in Figure 6 before melting is not known. One might also speculate if the drop in σ° later during the evening is surface-structure related rather than based on free-water content. In any case, these results point to the need for careful characterization of snow parameters.

Notwithstanding the uncertainties attributed to surface structure, and the requirement to measure free-water content in narrow layers close to the surface,

all measured reductions in backscatter coefficient $\Delta\sigma^\circ$ at 98 GHz were plotted against the percentage of free water to obtain proportionality factors. Straight lines were fitted to the data with the constraint that they pass through the origin ($\Delta\sigma^\circ$ = 0dB for FWC = 0%). The regression lines average at $\Delta\sigma^\circ_{VV} = 0.5$ FWC and $\Delta\sigma^\circ_{HV}$ = FWC with $\Delta\sigma^\circ$ in dB and FWC in percent.

Finally, we consider the 140-GHz data collected on 10 March (Figure 29) and

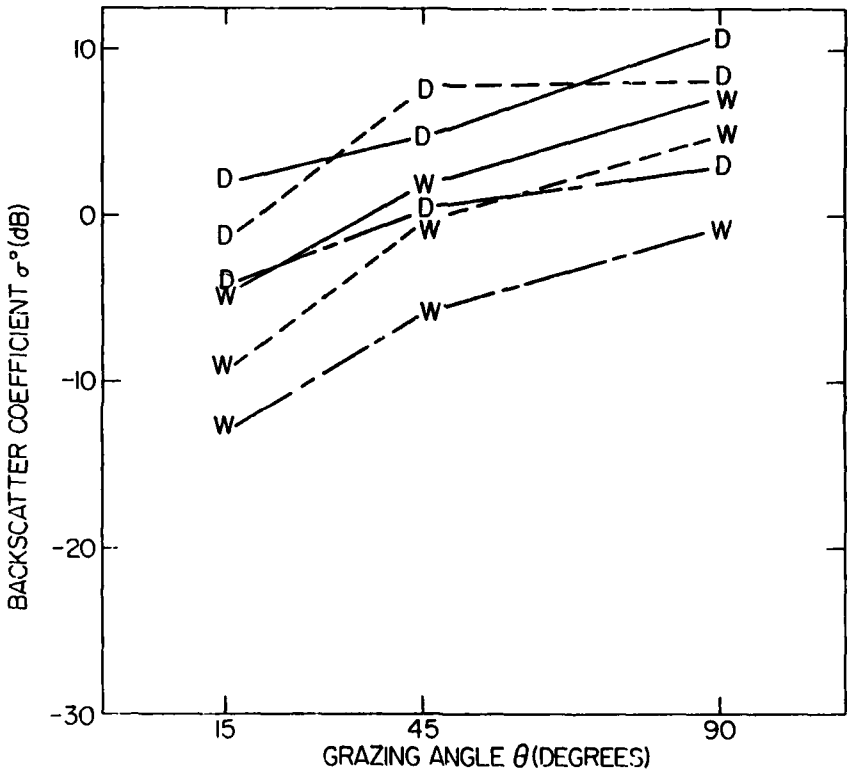

Figure 29. σ° vs Grazing Angle (10 March 1978, 140 GHz; Dry Snow, Polarization VV D—D, HH D- - -D, HV D-.-.-D; Wet Snow, Polarization VV W—W, HH W- - -W, HV W-.-.-W; Free-Water Content 5 Percent)

18 March (Figure 30). Of all frequencies, the highest backscatter coefficients were measured at 140 GHz. For instance, in Figure 29, σ°_{VV} at 90 deg is in excess of 10 dB on 10 March. At the same time, the effect of free water was the

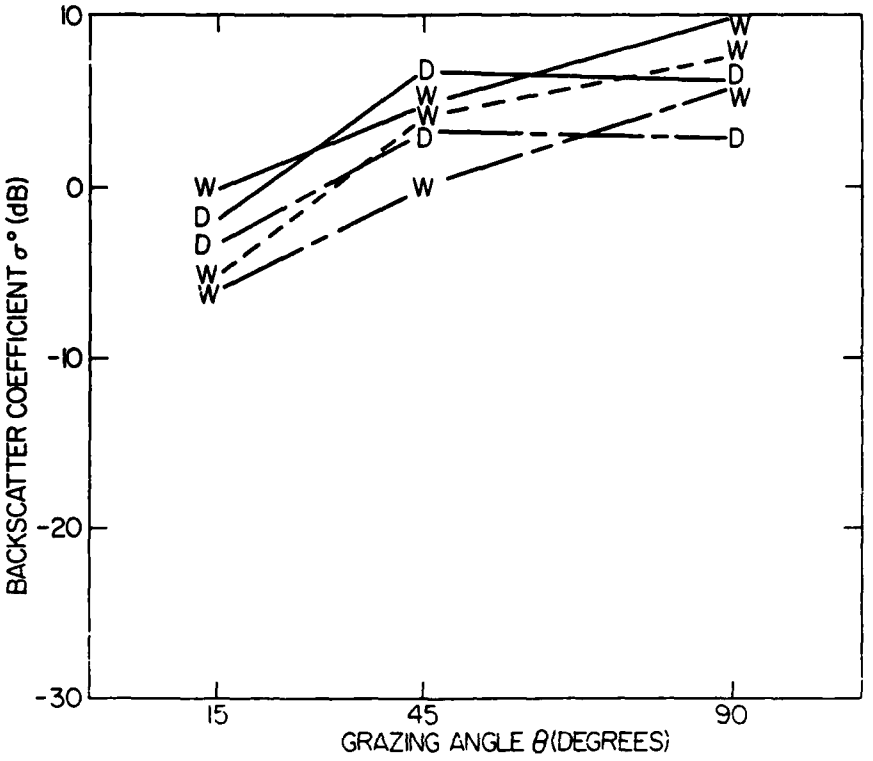

Figure 30. σ° vs Grazing Angle (18 March 1978, 140 GHz; Dry Snow, Polarization VV D—D, HV D-.-.-D; Wet Snow, Polarization VV W—W, HH W- - -W, HV W-.-.-W; Free-Water Content 8 to 11 Percent)

lowest at this frequency. With a free-water content of 5 percent, the drop in σ° ranged from 3 to 6 dB. Similar to the situation at 98 GHz but unlike that at 35 GHz, the nature of the σ°-curve did not change significantly between dry and wet snow.

Recall that, on 10 March, crusty, old snow formed the melting top layer, whereas on 18 March (Figure 30), the upper portion of the snow had been deposited only two days earlier and was essentially fresh. The 140-GHz data on these two days reinforce the trend seen already for the corresponding 98-GHz results. The spread of curves is substantially less on the second day. Closer inspection reveals that this impression is mostly due to the higher cross-polarized backscatter coefficient observed on the loose, wet snow. Unfortunately, only the curve for vertically polarized σ° exists for dry snow of 18 March. Note the remarkable fact that it lies below the associated wet-snow curves on this day.

Averages of 140-GHz measurements are plotted in Figure 31. Although these

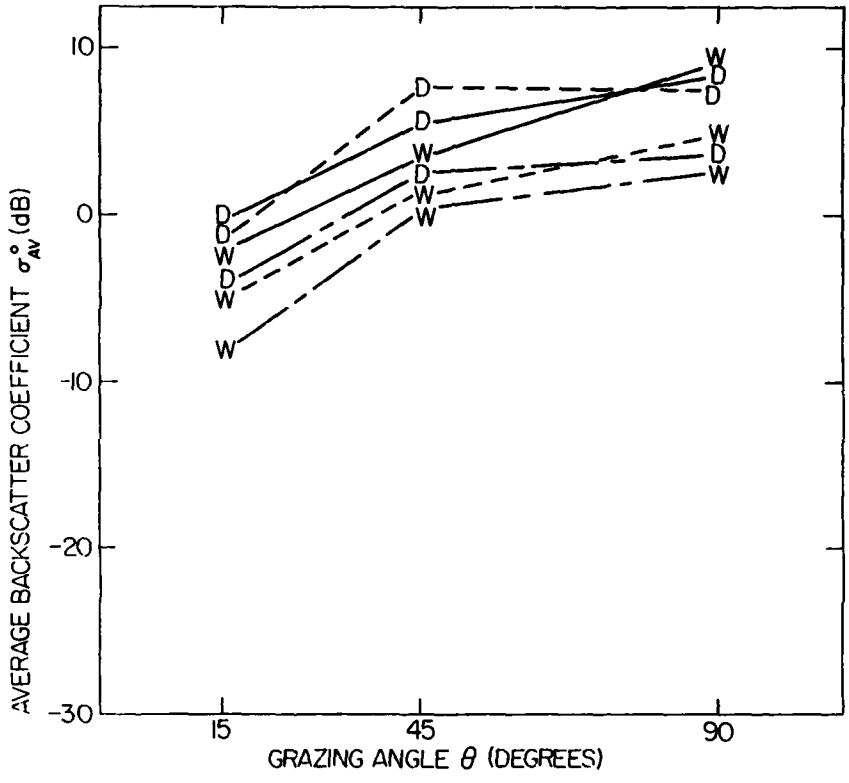

Figure 31. Average of σ° for All In-Situ Data (140 GHz, Dry Snow, Polarization VV D—D, HH D- - -D, HV D-.-.-D; Wet Snow, Polarization VV W—W, HH W- - -W, HV W-.-.-W; Free-Water Content 3 to 11 Percent)

curves are based on a range of snow structures and free-water percentages, like the 98-GHz averages in Figure 26 and the 35-GHz averages in Figure 23, systematic dependences on grazing angle and frequency are quite apparent by comparison. These are:

(a) Most angular variations of σ° are comparable to the ones postulated by the rough-surface scatter model.[8]

(b) A specular behavior is seen only over wet snow at 35GHz, where it is quite pronounced. Some indications of specular scatter may have been lost in the three-point sampling of the actual curves. Specular contributions had been found in the continuous angular scans over frozen sleet up to 140 GHz.[8] The 98-GHz wet-snow curve of σ°_{VV} resembles the specular ones. It is out of

line with the σ°_{HH} and the corresponding higher-frequency curves, which places the 15-deg value in some doubt.

(c) The cross-polarized component changes drastically at 35 GHz as the snow becomes wet, less at 98 GHz, and almost not at all at 140 GHz.

(d) The differences between vertical and horizontal polarization do not permit one to draw systematic conclusions, although there is an indication of σ°_{HH} dropping more rapidly with grazing angle than σ°_{VV}.

For a better appreciation of their frequency dependence, σ°_{VV} and σ°_{HV} have been redrawn from Figures 23, 26, and 31. In Figures 32 to 34, the results

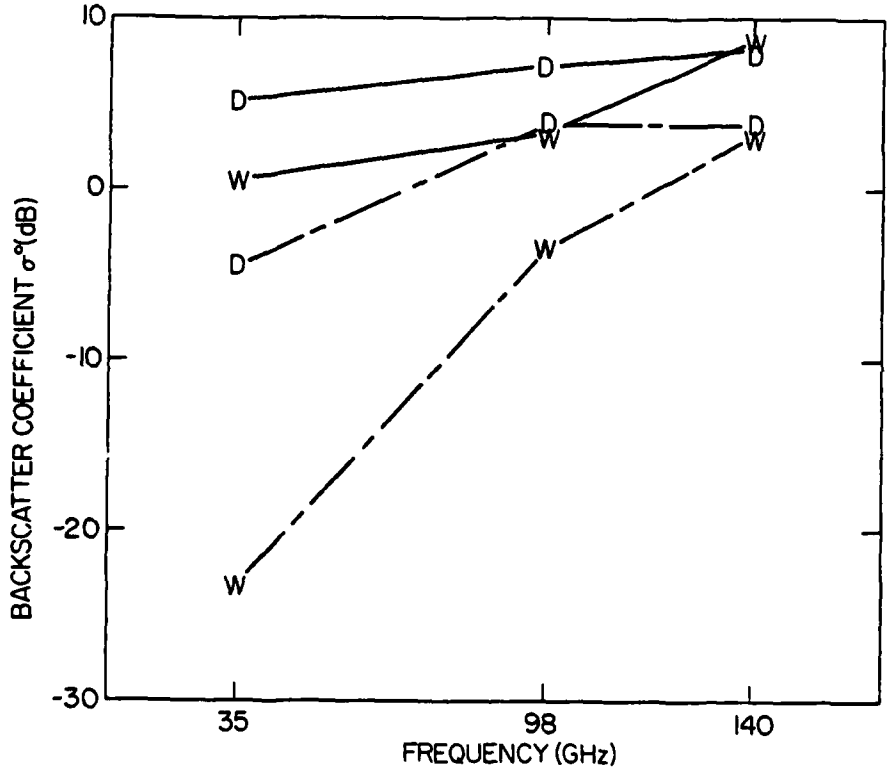

Figure 32. Average σ° vs Frequency, Grazing Angle of 90 deg (Dry Snow, Polarization VV D—D, HV D-.-.-D; Wet Snow, Polarization VV W—W, HV W-.-.-W)

are shown for one grazing angle each, with frequency as the independent variable. The increase of all backscatter coefficients with frequency is obvious. A minor

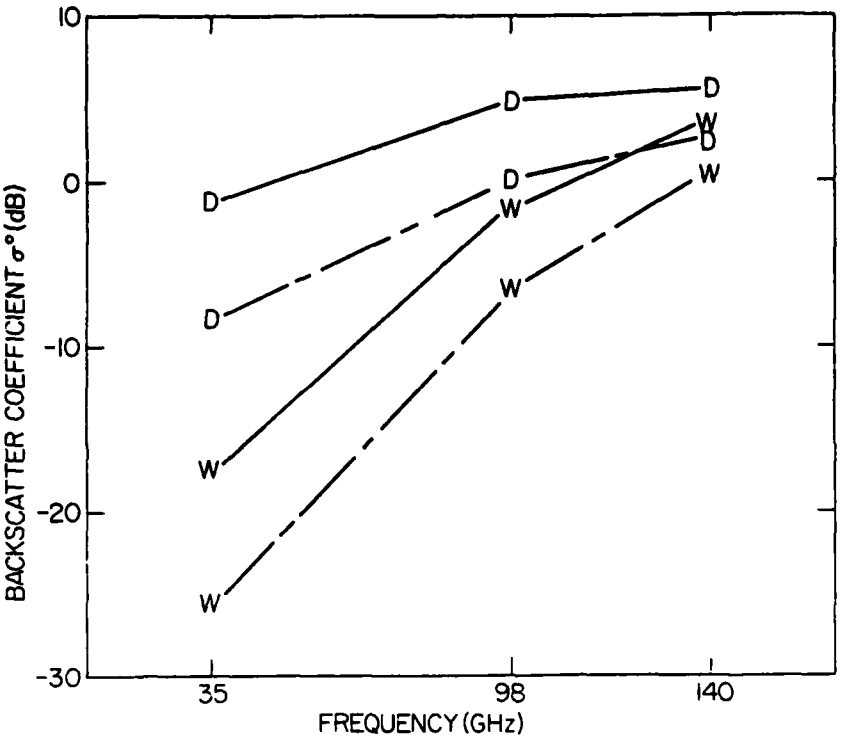

Figure 33. Average σ° vs Frequency, Grazing Angle of 45 deg (Dry Snow, Polarization VV D—D, HV D-.-.-D; Wet Snow, Polarization VV W—W, HV W-.-.-W)

deviation is σ°_{VV} at 15 deg between 98 and 140 GHz. At all grazing angles, differences between like- and cross-polarization or between dry and wet snow decrease with increasing frequency. In the majority of cases, the rate of σ°-increase drops with frequency. Frequency is plotted on a linear scale.

4.4 Comparison With Related Experiments

Probably the earliest measurements of the backscatter properties of snow were conducted by Cosgriff, Peake, and Taylor.[12] They measured the backscatter ceofficients of different types of terrain with and without snow cover. Measurements were made at 10, 15.5, and 35 GHz, and at grazing angles ranging from 10

12. Cosgriff, R.L., Peake, W.H., and Taylor, R.C. (1960) Terrain Scattering Properties for Sensor System Design (Terrain Handbook II), Engineering Experiment Station Bulletin 181, The Ohio State University.

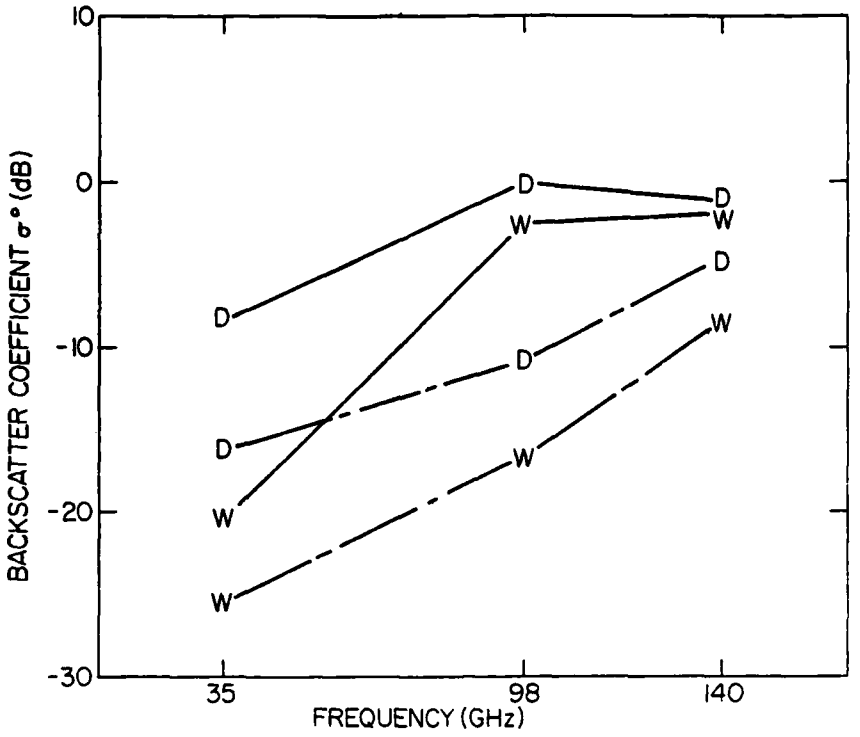

Figure 34. Average σ° vs Frequency, Grazing Angle of 15 deg (Dry Snow, Polarization VV D—D, HV D-.-.-D; Wet Snow, Polarization VV W—W, HV W-.-.-W)

to 80 deg. They found that, at 35 GHz, dry snow cover led to an increase in the backscatter coefficient over the coefficient from bare terrain. Wet snow caused the coefficient to decrease. Qualitatively, these results agree with ours. Cosgriff et al gave insufficient ground truth data to allow a quantitative comparison. They recorded only the air temperature and snow depth.

Hoekstra and Spanogle[2] determined the backscatter properties of snow and ice at 10, 35, and 95 GHz. Measurements were made only over the narrow range of grazing angles between 0.3 and 1 deg. This is well outside our range, 15 to 90 deg, and thus precludes a meaningful comparison of the data. They do report 10-GHz backscatter cross-sections showing a rapid drop when the snow cover contained free water. This is in qualitative agreement with our results.

Currie[6] and his coworkers of the Georgia Institute of Technology conducted a series of field measurements on the backscatter and attenuation properties of snow at Steamboat Springs, Colorado, in 1976. The backscatter coefficient of dry

and wet snow was determined with pulse radars at 35 and 95 GHz. We discussed their attenuation measurements in our snow-slab report.[8] Their backscatter measurements were made at 15-deg grazing angle. Typical results are shown in Table 5. Note that the values given for σ° are termed peak values. Currie did

Table 5. Typical Values of σ° Measured at Grazing Angle of 15 deg by Georgia Institute of Technology[6]

Snow Type	Frequency (GHz)	Typical Peak Values of σ°	
		Parallel Polarization	Cross Polarization
Frozen Metamorphic Snow	35	-8dB	-18dB
	95	<-10dB	<-10dB
Wet Metamorphic Snow	35	-15dB	-28dB

not specify whether these are the peaks of the fluctuating backscatter signal as in our analysis. He did report, in agreement with our results, that their data were best matched by a lognormal distribution. Their 35-GHz data, except the like-polarized data from wet, metamorphic snow, agree quite well with ours. Measurements at 95 GHz were limited by the sensitivity of their radar. Therefore, backscatter coefficients were obtained only for frozen snow. Their conclusion was that σ° at 95 GHz is less than that at 35 GHz. Our Figure 34 shows just the opposite. Currie did not state the orientation at which the parallel polarization measurements were made.

The most comprehensive investigations in the microwave region on snow were made by Ulaby's group at the University of Kansas.[1,3,4,5] In 1975, they measured backscatter properties of snow over the 1- to 8-GHz range.[1] During these tests, the snow depth was typically 12 to 15 cm. Dry snow had practically no effect on the backscatter coefficient compared with the effect of bare ground. An appreciable change was discovered when the snow contained free water. They conducted an extended series of measurements in 1977.[3,4] These tests were performed in Steamboat Springs, Colorado, at frequencies ranging from 1 to 18 GHz and at 35 GHz. Grazing angles of 20 to 90 deg were covered. In addition, radiometric measurements were carried out at 10.69, 37, and 94 GHz.

Our results complement those of Ulaby et al.[1,3,4,5] They can be compared at the one frequency we have in common, 35 GHz. Otherwise, there is no overlap in the data. The snow at their test site differed from our snow in a number of

ways. The average density at Steamboat Springs varied from 0.21 to 0.30g/cm^3. Ours ranged from 0.28 to 0.43g/cm^3. Grain sizes at their test site were smaller. At Hanscom AFB, snow-grain diameters were never less than 1 mm, and, in most cases, they were larger. Due to the MF conditions during our tests, the particles were bonded together to form quite large conglomerates (Figure 9). Metamorphism apparently took place at Steamboat Springs through a slow equitemperature process, as Ulaby et al report grain sizes near the surface between 0.25 and 0.5 mm. Only on the last day did they find particles at the surface ranging from 1 to 2 mm in diameter. Apparently, snow melt at Steamboat Springs was less severe than snow melt during our tests. The peak wetness reported by Ulaby et al was 4.5 percent. Wetness was measured in the top 5-cm layer of snow. Down to the same depth, we found a wetness as high as 14.7 percent. A maximum of 17.4 percent was measured in the upper 7.5-cm layer on 11 March. The differences in snow parameters should be kept in mind when comparing results.

Figure 8-7 of Stiles and Ulaby[5] shows one set of σ^o-data as a function of grazing angle and polarization over dry and wet snow at 35 GHz. Wet-snow measurements on 19 February 1977 were followed by dry-snow measurements the next morning. In Figures 35 and 36, we have replotted them along with our σ^o-averages at 35 GHz. Stiles and Ulaby determined larger σ^o than we did. Their values exceed ours for dry snow by between 4 and 10 dB, depending on grazing angle and polarization. For wet snow, differences cover about the same range if we consider like polarization. Cross-polarized backscatter coefficients differ by as much as 20 dB and more. Both sets of data display the decrease in σ^o and a pronounced specular response with grazing angle as water forms in the snow.

We attribute the observed σ^o-difference predominantly to snow structure. The deviation between corresponding data points becomes larger for lower grazing angles. This is qualitatively explained by the less dense, small-grained Colorado snow which follows the volume scatter model[8] better than the Massachusetts snow. Massachusetts snow is a better surface scatterer. The Colorado snow must also have presented a less mirror like water surface during melting or the cross-polarized backscatter could not have been sustained at the level shown.

Stiles and Ulaby[5] discuss the backscatter response to grazing angle and free-water content over the whole lower frequency range they examined. We repeat their conclusions (in quotation marks) and compare them with our own findings at the higher frequencies as follows:

(a) "Snow wetness has a minor effect on σ^o at 2.6 GHz. The sensitivity to wetness increases with frequency."

Our measurements at 35 GHz show a stronger sensitivity of σ^o to snow wetness than the University of Kansas data. We see the sensitivity decreasing again at 98 and 140 GHz.

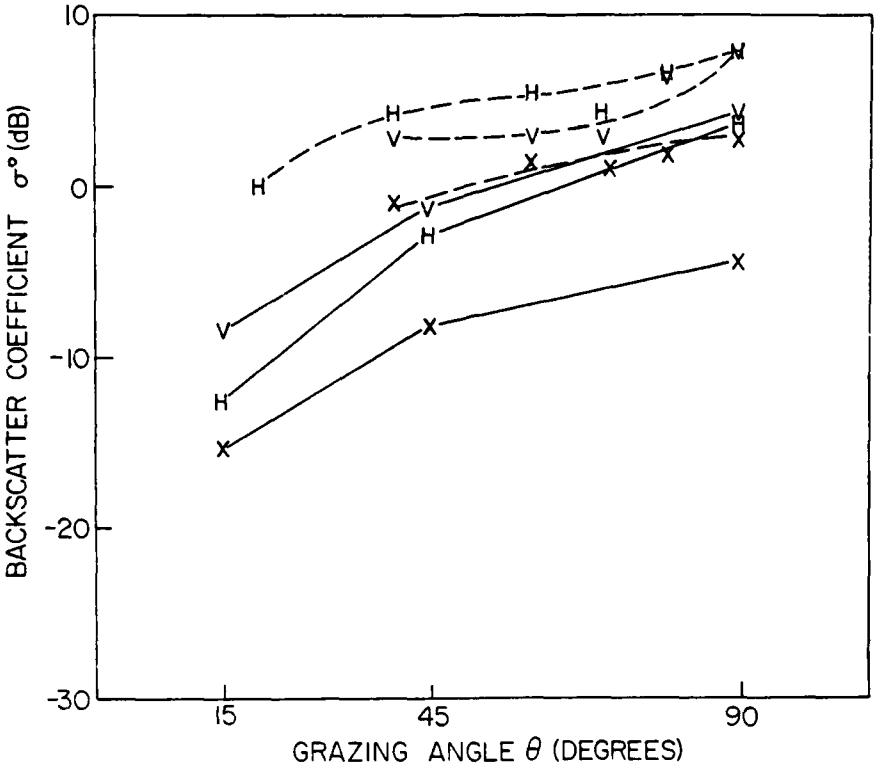

Figure 35. Comparison of σ° Measured by University of Kansas at 35 GHz - - - With Our Average σ° for Dry Snow ——— Taken from Figure 23

(b) "The sensitivity of σ° to wetness generally increases with increasing angle of incidence and results in a lowering of σ° at angles away from nadir."

Our results are in agreement.

(c) "The rate of increase of σ° with frequency is greater for dry snow than for wet snow at angles away from nadir."

The situation is reversed in our case. The rate of increase with frequency is greater for wet than for dry snow. This is also true at nadir.

(d) "The depolarization ratio of σ° increases with frequency to approximately -2dB at 35 GHz and 50 deg, indicating a volume scatter mechanism at the higher frequencies."

The depolarization ratio is defined[5] as $\sigma^\circ_{HV} / \sigma^\circ_{VV}$. Our data for dry snow show a growing depolarization ratio with frequency. However, we measure a

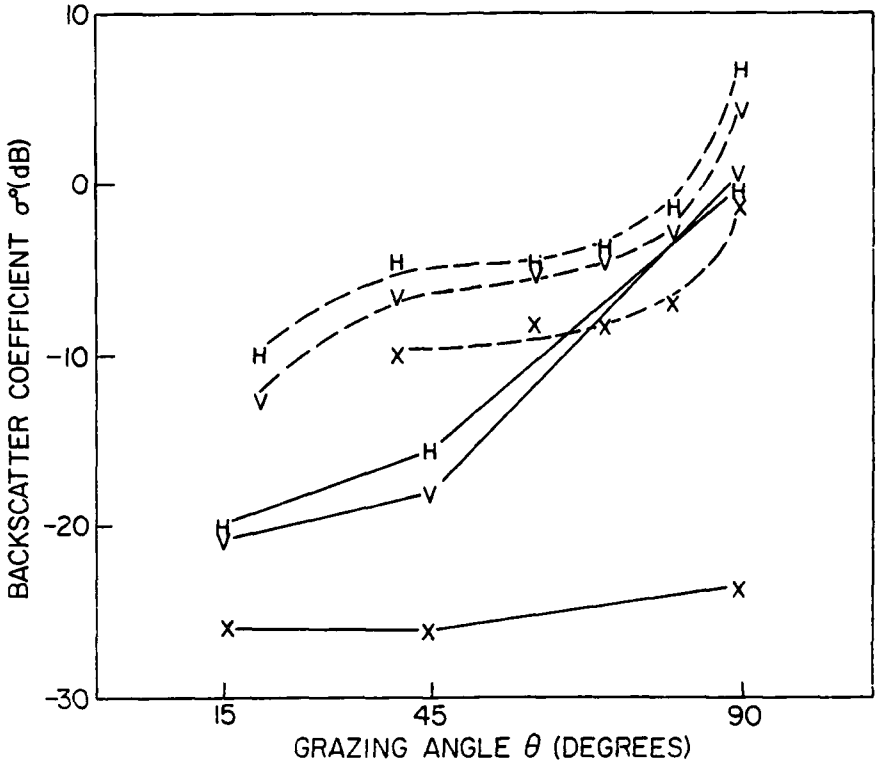

Figure 36. Comparison of σ° Measured by University of Kansas at 35 GHz - - - With Our Average σ° for Wet Snow ——— Taken from Figure 23

smaller depolarization ratio at 35 GHz (-7dB at 45 deg). The corresponding values are -5dB at 98 GHz and -3 dB at 140 GHz.

(e) "The scatter mechanism seems to vary. For wet snow, σ° is governed by surface scatter at all frequencies. For dry snow, volume scattering is responsible for the σ°-behavior at the higher frequencies and soil contributions are important at the lower frequencies."

Our data gave no indication of soil influence. At 35 GHz, the angular response drops off more rapidly than predicted by either rough-surface or volume scattering. At the higher frequencies, the drop is closer to that predicted by these two models, but it is not possible to distinguish between them.

(f) "Surface roughness effects are relatively minor (less than 3 dB) when the

snow is dry."

The same conclusion can be drawn from our results.

(g) "Surface roughness is very important when wetness is present."

Our measurements at 90 deg showed a higher return from wet snow whose surface was relatively smooth (compare data of 10 March and 18 March). However, at other grazing angles, we saw no effect.

(h) "The dynamic range of σ° due to wetness increases with frequency from about 0 dB at 1.2 GHz to as much as 15 dB at 35 GHz (for 50 deg of incidence) in response to an m_v change from 0% to greater than 1.3%."

Here m_v is the free-water content by weight. Our data agree at 35 GHz. At this frequency, we measured at 45 deg an average decrease of 16 dB for σ°_{VV} and 12 dB for σ°_{HH} due to snow wetness. The sensitivity to free water goes down at the higher two frequencies. The reduction in backscatter coefficient at 98 GHz is 6 dB for σ°_{VV} and 4 dB for σ°_{HH}. At 140 GHz, the corresponding numbers are 2 dB and 6 dB.

(i) "This dynamic range decreases as θ approaches nadir."

Our results agree.

(j) "The time rate of change of σ° increases with increasing frequency. This phenomenon is related to the decreasing penetration depth with increasing frequency and the faster possible rate of change of m_v in the thinner layer to which the higher frequency σ° values respond."

We did not obtain sufficient diurnal information at 35, 98, and 140 GHz to determine response times. However, we see no reason why this conclusion should not apply in our frequency regime.

(k) "σ° response to wetness is linear at low frequencies but becomes non-linear at the higher frequencies."

At 35 GHz, Stiles and Ulaby assume that σ° is sensitive to free water in a top layer much thinner than 5 cm, their standard snow sampling depth. The observation of a "non-linear" dependence of σ° on wetness is attributed to water saturation in this sensitive top layer, which coincides with an average 5-cm free-water content as low as 1 percent. In effect, the rate of σ° decrease is high until 1 percent of average free water is reached, and much lower beyond this level.

Our snow sampling depths, necessitated by the calorimetric equipment, most likely were not matched too well with the depth of millimeter-wave/snow interaction either. There is reason to assume that near-surface parameters are even more relevant at 98 and 140 GHz than at 35 GHz.

(l) "A hysteresis effect is seen between σ° and m_v in the top 5 cm layer. The effect is related to the fact that the response is governed by the complete snow profile and the characterization by the wetness in the top 5 cm layer has varying validity."

Again, "hysteresis" appears to exist because the wetness of the directly interacting layer could not be measured. We may have seen a similar effect during the period of exclusive 98-GHz measurements on 11 March 1978. The measurements on dry snow[8] with presumably greater penetration indicated that σ° varied little when a slab of 12.5-cm thickness was reduced to 2.5 cm.

(m) "The correlation coefficient and sensitivity of σ° to changes in m_v became more negative with increasing frequency and angle of incidence."

Our 35-GHz data suggest a similar dependence on θ. However, at 98 and 140 GHz, it is not clear that free-water effects change the same way with angle. We definitely observe a frequency dependence above 35 GHz reversed from the one found by Stiles and Ulaby.

5. CONCLUSIONS

Backscatter measurements at 35, 98, and 140-GHz over undisturbed in-situ snow cover were conducted to study the effect of liquid water on the millimeter-wave backscatter coefficient, and to complement previous results on frozen snow slabs.[8] Since relatively steep depression angles appeared to be of interest from an applications viewpoint, grazing angles of 90, 45, and 15 deg were selected. Comparability of the slab measurements and dynamic-range limitations in the instrumentation contributed to this choice. Although areas covered by individual measurements were substantially larger in the in-situ case than in the slab case, this was not an attempt at large-scale mapping or imaging of the snow surface which might be typical for an airborne radar system. The measurements were conducted over level terrain, and the snow appeared to be uniform within the region covered by the antenna beams. Backscatter data recorded during the circular sweeps of the 3-frequency scatterometer across the snow surface were therefore averaged over each sweep. Structurally, the snow varied from fresh to metamorphic, almost 4 weeks old. The total depth was never less than 30 cm. Based on attenuation coefficients measured on slabs, it appears that scatter from the underlying terrain can be neglected even at 35 GHz, where the deepest penetration occurred.

During the test period, the snow was usually frozen solid before sunrise. Within 1 or 2 hours after sunrise, free water could be detected. A melting-water calorimeter provided the free-water data reported here. It must be understood that measuring free-water content by fractional weight and interpreting its effect on backscatter is difficult. As indicated in the body of the report, free-water generation in the snow and vertical transport of free water through the snow is a complicated process. The need to probe snow consistency within narrow layers is

somewhat in conflict with the requirement for substantial quantities of snow in order to reduce calorimeter error. Free-water concentrations as measured show some nonsystematic variation, and, hence, scatter when correlated with backscatter coefficients. The adequate characterization of wet snow is a problem in other areas of research, too. Notwithstanding these limitations, the general trends observed for the influence of meltwater on snow backscatter are believed to be correct.

In summary, the increase in the like-polarized backscatter coefficient with frequency, found during the slab measurements on dry snow, was confirmed at all grazing angles. Values ranged from a minimum of -9dB at 35 GHz and 15-deg grazing angle to well over 0dB at all frequencies (8dB to 140 GHz) at 90-deg grazing angle. The cross-polarized backscatter coefficient, following the same general trend, spread from a low of -16dB at 35 GHz and 15 deg to a high of 2dB at 140 GHz and 90 deg. With increasing frequency, volume or rough-surface scatter appeared to prevail over specular reflection. This was also apparent when liquid water formed in the snow. While in almost all cases like-polarized backscatter coefficients were lower for wet snow than for dry snow, the drop became less significant with higher frequency. Actually, at 140 GHz and perpendicular incidence, no reduction was found. Cross-polarized backscatter coefficients of wet snow at 90-deg grazing angle ranged from a low of -24dB at 35 GHz to a high of 0dB at 140 GHz. At lower grazing angles, the change was somewhat less dramatic. Overall, the frequency dependence for wet snow was more pronounced than for dry snow.

References

1. Ulaby, F.T., Stiles, W.H., Dellwig, L.F., and Hanson, B.C. (1977) Experiments on the radar backscatter of snow, IEEE Trans. on Geoscience Electronics, GE-15 (No. 4): 185-189.
2. Hoekstra, P., and Spanogle, D. (1972) Backscatter from snow and ice surfaces at near incident angles, IEEE Trans. on Ant. and Prop., AP-20 (No. 6): 788-790.
3. Stiles, W.H., Hanson, B.C., and Ulaby, F.T. (1977) Microwave Remote Sensing of Snow, Experiment Description and Preliminary Results, University of Kansas RSL Tech. Rep. 340-1.
4. Ulaby, F.T., and Stiles, W.H. (1978) The Active and Passive Microwave Response to Snow Parameters. Part I: Wetness Part II: Water Equivalent of Dry Snow, University of Kansas RSL Tech. Rep. 340-2.
5. Stiles, W.H., and Ulaby, F.T. (1980) Microwave Remote Sensing of Snowpacks, NASA Contr. Rep. 3263, Contract NAS5-23777.
6. Currie, N.C. (1977) Private communication.
7. Ulaby, F.T., Fung, A.K., and Stiles, W.H. (1978) Backscatter and Emission of Snow: Literature Review and Recommendations for Future Investigations, University of Kansas RSL Rep. 369-1.
8. Lammers, U.H.W., Hayes, D.T., and Marr, R.A. (1981) Millimeter Wave Scatter and Attenuation Measurements on Snow Slabs, RADC-TR-81-88, AD A112595.
9. Marshall, J.S., and Hitschfeld, W. (1953) Interpretation of the Fluctuating Echo from Randomly Distributed Scatterers, Part I, Can. J. Phys. 31:962-94.
10. Ruina, J.P. (1963) The fluctuation of radar ground return due to antenna scanning, IEEE Trans. on Ant. and Prop. AP-11(No. 6):722-723.
11. Gumbel, E.J. (1958) Statistics of Extremes, Columbia University Press, New York.

12. Cosgriff, R. L., Peake, W. H., and Taylor, R. C. (1960) Terrain Scattering Properties for Sensor System Design (Terrain Handbook II). Engineering Experiment Station Bulletin 181, The Ohio State University.

Appendix A

Snow Data

Physical parameters of the snow cover are presented in this section. One combination table/diagram is given for every day that millimeter-wave measurements were conducted (Tables A1 through A6). The data shown in these tables characterize the snow before the time the millimeter-wave measurements were begun. A standard form of presentation has been used. The vertical scale at the center of the form gives the height above ground. The stratigraphy of the snow cover is shown by horizontal lines drawn between the left edge of the form and the height scale. Most of the column headings are self-explanatory. The "Layer" column normally contains a brief description of the layer such as hard, icy, slightly wet, etc. In the "Density" column, a tick mark is placed to show the height at which the measurements were made. The air temperature, indicated by the symbol $\oplus$ on the temperature plot, was obtained at a position just above the surface of the snow. The "Comments" column includes such information as surface hardness, weather data, data on the history of the snow, and, in some cases, additional information on the stratigraphy of the snow. The snow was mostly frozen when the pre-dawn data shown in Tables A1 through A6 were collected.

A corresponding set of tables (A7 through A9) contains the diurnal variation of snow and air temperatures as well as the change in free-water content. These data were recorded at intervals of one-half hour or greater, as the change in conditions warranted. "Depth of Sample" means that snow from the surface down to the indicated level was used to determine the free-water content.

Table A1. Physical Parameters of Snow Cover 10 March 1978

LAYER	GRAIN TYPE	GRAIN SIZE (mm)	DENSITY (g/cm^3)	HEIGHT (cm)
Crust	Rounded	1 Some as large as 2		40
Icy Crust	Rounded	as above	0.28	35
Loose Snow	Rounded	1 Some as large as 2		30
			0.31	25
				20
				15
Ice				10
				5
				0

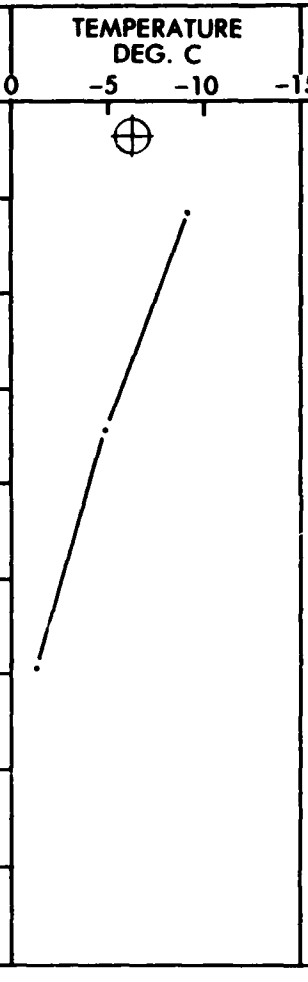

COMMENTS

Average surface hardness: 4166 g/cm^2

In crust, grains are frozen together. Structure has many air pores.

In icy crust, grains are frozen together. Structure has few air pores.

Sky was overcast throughout runs, radiational melting was minimal.

Table A2. Physical Parameters of Snow Cover 11 March 1978

LAYER	GRAIN TYPE	GRAIN SIZE (mm)	DENSITY (g/cm^3)
Crusty	Rounded	1	
Crusty and Icy	Rounded	1 Some as large as 4	0.28
Icy	Rounded		
Loose Snow	Rounded	1	0.31
Ice			

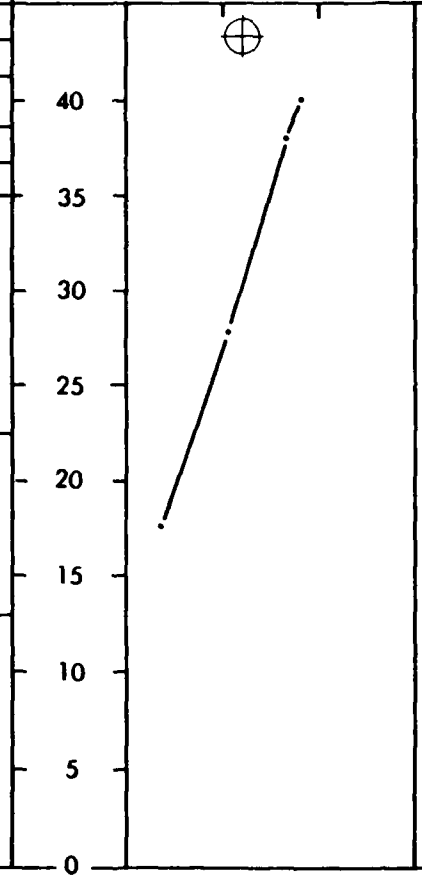

COMMENTS

Average surface hardness: 2500 g/cm^2

Snow depth in front of scatterometer is 40 cm.

0500 Air temperature -4°C
0650 Perfectly clear sky, sun 10 deg above horizon
1030 Clear, no wind
1230 Clear, light breeze
1315 Clear, breezy
1405 Slightly overcast, gusty winds
1600 Slightly overcast, strong gusty winds
1700 Slightly overcast, gusty winds
1800 Sunset, cloudy, breezy
1900 Sky mostly clear. Snow can be easily made into ball. Squeezing it produces no visible water.
2000 High clouds
2030 Air temperature 3°C
2050 Air temperature 3°C, breezy

Table A3. Physical Parameters of Snow Cover 13 March 1978

LAYER	GRAIN TYPE	GRAIN SIZE (mm)	DENSITY (g/cm^3)	HEIGHT (cm)	TEMPERATURE DEG. C (0, -5, -10, -15)	COMMENTS
				40		
				35	⊕	Surface hardness: 7000 g/cm^2.
Hard	Rounded	1 and 2 Particles bonded together in solid mass	0.36	30		0550 Clear, sun just below horizon. Air temperature -2°C.
				25		0624 Sunrise
Soft Slush	Rounded	1 Particles bonded together, mean size 2 to 3, many as large as 5	0.43	20		0700 Clear, calm with a few high cirrus clouds.
				15		1315 Snow condition: 13 cm ice on ground, 18 cm wet snow on top of ice.
Ice				10		
				5		
				0		

Table A4. Physical Parameters of Snow Cover 14 March 1978

LAYER	GRAIN TYPE	GRAIN SIZE (mm)	DENSITY (g/cm^3)	HEIGHT (cm)	TEMPERATURE DEG. C (0, -5, -10, -15)	COMMENTS
				40		
				35		
				30		
Hard	Rounded	1 and 2 Particles bonded together, many as large as 5	0.39	25		Surface hardness: 5600 g/cm^2
				20		0530 High clouds, overcast 0630 Air feels quite damp after sunrise 0700 Solid overcast, light wind 1000 Measurements stopped. Cold and windy, overcast
Slush	Rounded	As above but not bonded together	0.53	15		Depth of snow at base of scatterometer is approx. 30 cm.
Ice				10		
				5		
				0		

Table A5. Physical Parameters of Snow Cover 18 March 1978

LAYER	GRAIN TYPE	GRAIN SIZE (mm)	DENSITY (g/cm^3)	HEIGHT (cm)	TEMPERATURE DEG. C (0, -5, -10, -15)	COMMENTS
				40		On 16 March, 15 to 20 cm of powdery snow was deposited.
				35		
Loose Snow				30		0400 Clear skies, T_{air} = -10°C
				25		0815 T_{air} = -3.5°C, snow still very dry and powdery. Clear skies, no wind.
				20		1020 Cannot make snow ball with new snow.
Snow	Rounded	1 to 2		15		1100 Can make snow ball. Snow will hardpack, but no water can be squeezed out of it.
				10		1300 Scattered fair weather clouds obscure sun from time to time.
Ice				5		1340 Windy
				0		1415 High winds but mainly sunny.

Table A6. Physical Parameters of Snow Cover 20 March 1978

LAYER	GRAIN TYPE	GRAIN SIZE (mm)	DENSITY (g/cm^3)
Hard	Rounded	1 to 2 grains bonded together. Some as large as 3 to 5	0.39
Slightly Wet	Rounded	As above, grains not bonded together	
Ice			

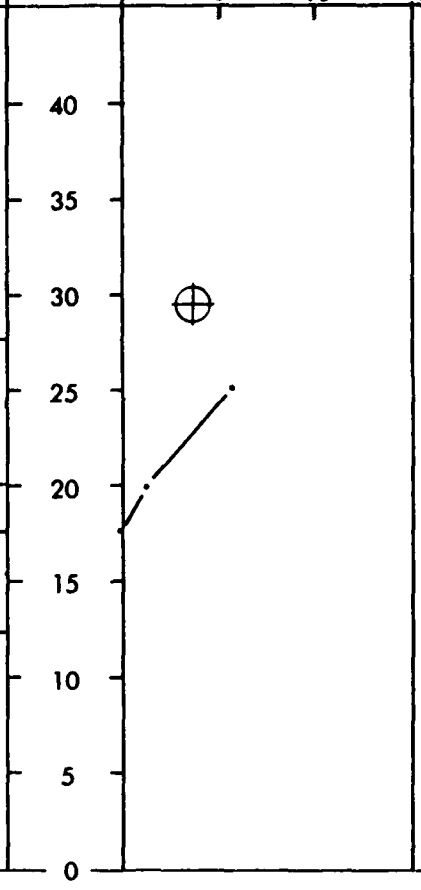

COMMENTS

Surface hardness: 6875 g/cm^2.

0500 Clear skies, T_{air}=-2.5°C
0620 Sunrise
0715 Clear skies, slight wind

Snow test area contains scattered cup indentations on surface. This resulted from the melting on 19 March.

Snow depth in test area (down to top of ice layer) ranges from 10 to 15 cm. Large patches of ice (several meters across) can be seen beyond test area.

Table A7. Free-Water Content of Snow Cover 10 March 1978

RUN NO.	TIME	DEPTH OF SAMPLE (cm)	H_2O CONTENT (% wt.)	AIR TEMP (°C)	SNOW TEMP. BELOW SURFACE(cm)				
					2.5	5.0	7.5	12.5	15.0
1	0720	12.5	1.3						
2	0745	12.5	1.7						
3	0815	12.5	1.6						
4	0900	12.5	1.8						
5	1000	12.5	1.8						
6	1115	12.5	1.8	8.0	-3.0		-2.0		-2.0
7	1200	5.0	4.7	5.0	-1.5		-1.5		-1.5
8	1330	12.5	10.0	2.0	-0.5		-0.5		-1.0
9	1415	5.0	5.8	6.0	-0.5		-0.5		-1.0
10									
11									
12									
13									
14									
15									
16									
17									
18									
19									
20									
21									

Table A8. Free-Water Content of Snow Cover 11 March 1978

RUN NO.	TIME	DEPTH OF SAMPLE (cm)	H_2O CONTENT (% wt.)	AIR TEMP (°C)	SNOW TEMP. BELOW SURFACE(cm)				
					2.5	5.0	7.5	12.5	15.0
1	0700	5.0	0.1	-3.0	-9.0	-9.0			-5.0
2	0730	5.0	3.0	-2.0	-8.0	-8.0			-5.0
3	0815	5.0	1.2	0.0					
4	0850	5.0	1.5	3.0	-5.0	-6.0			-6.0
5	0930	5.0	2.0	3.0	-2.0	-4.0			-4.0
6	1045	2.5	10.1	4.0	0.0	-1.0			-4.0
7	1115	2.5	16.0	5.0	0.0	-2.0			-3.0
8	1145	5.0	12.5	4.0	1.0	-1.0			-3.0
9	1330	7.5	17.4	4.0	0.0	0.0			-2.0
10	1400	12.5	15.5	2.0	0.0	0.0			-2.0
11	1500	20.0	12.1	6.0	0.0	0.0			-1.0
12	1615	20.0	9.0	5.0	0.0	0.0			-1.0
13	1730	20.0	9.7	5.0	0.0	0.0			-1.0
14	1915	2.5	8.8						
15	2125	2.5	6.7						
16									
17									
18									
19									
20									
21									

Table A9. Free-Water Content of Snow Cover 18 March 1978

RUN NO.	TIME	DEPTH OF SAMPLE (cm)	H_2O CONTENT (% wt.)	AIR TEMP (°C)	SNOW TEMP. BELOW SURFACE (cm)				
					2.5	5.0	7.5	12.5	15.0
1	0805	5.0	1.4	-4.0		-3.0			
2	0830	5.0	1.1	-3.0		-2.0			
3	0855	5.0	0.6	-3.0		-2.0			
4	0925	5.0	1.7	-2.0		-2.0			
5	0955	5.0	0.1	0.0		-2.0			
6	1025	5.0	2.0	0.0		-2.0			
7	1050	5.0	1.6	1.0		-2.0			
8	1120	2.5	3.1	1.0		-1.0			
9	1150	2.5	5.3	0.0		-1.0			
10	1220	2.5	4.8	0.0		-1.0			
11	1325	2.5	10.7	-1.0		-2.0			
12	1355	2.5	8.4	-1.0		-1.0			
13	1425	2.5	10.7	2.0		-1.0			
14	1500	2.5	9.1	1.0		-1.0			
15	1530	2.5	7.4	0.0		-1.0			
16	1615	2.5	5.5	-1.0		-1.0			
17									
18									
19									
20									
21									

MISSION
of
Rome Air Development Center

RADC plans and executes research, development, test and selected acquisition programs in support of Command, Control Communications and Intelligence (C^3I) activities. Technical and engineering support within areas of technical competence is provided to ESD Program Offices (POs) and other ESD elements. The principal technical mission areas are communications, electromagnetic guidance and control, surveillance of ground and aerospace objects, intelligence data collection and handling, information system technology, ionospheric propagation, solid state sciences, microwave physics and electronic reliability, maintainability and compatibility.

Printed by
United States Air Force
Hanscom AFB, Mass. 01731

END

FILMED

10-84

DTIC